Recent progress in optoelectronic memristors for neuromorphic and in-memory computation

NEUROMORPHIC
Computing and Engineering

OPEN ACCESS

RECEIVED
6 February 2023

REVISED
5 April 2023

ACCEPTED FOR PUBLICATION
12 May 2023

PUBLISHED
25 May 2023

TOPICAL REVIEW

Recent progress in optoelectronic memristors for neuromorphic and in-memory computation

Maria Elias Pereira*, Rodrigo Martins, Elvira Fortunato, Pedro Barquinha and Asal Kiazadeh*

i3N/CENIMAT, Department of Materials Science, NOVA School of Science and Technology and CEMOP/UNINOVA, NOVA University Lisbon, Campus de Caparica, 2829-516 Caparica, Portugal

* Authors to whom any correspondence should be addressed.

E-mail: mel.pereira@campus.fct.unl.pt and a.kiazadeh@fct.unl.pt

Keywords: optoelectronic memristors (OEMs), photonic memristors, resistive switching devices, artificial neural networks (ANNs), artificial visual systems, neuromorphic computing

Abstract

Neuromorphic computing has been gaining momentum for the past decades and has been appointed as the replacer of the outworn technology in conventional computing systems. Artificial neural networks (ANNs) can be composed by memristor crossbars in hardware and perform in-memory computing and storage, in a power, cost and area efficient way. In optoelectronic memristors (OEMs), resistive switching (RS) can be controlled by both optical and electronic signals. Using light as synaptic weigh modulator provides a high-speed non-destructive method, not dependent on electrical wires, that solves crosstalk issues. In particular, in artificial visual systems, OEMs can act as the artificial retina and combine optical sensing and high-level image processing. Therefore, several efforts have been made by the scientific community into developing OEMs that can meet the demands of each specific application. In this review, the recent advances in inorganic OEMs are summarized and discussed. The engineering of the device structure provides the means to manipulate RS performance and, thus, a comprehensive analysis is performed regarding the already proposed memristor materials structure and their specific characteristics. Moreover, their potential applications in logic gates, ANNs and, in more detail, on artificial visual systems are also assessed, taking into account the figures of merit described so far.

1. Introduction

It is becoming increasingly urgent to find an alternative to the long-time used Von Neuman architecture, in which the bottleneck of transferring data between the processor and the memory unit remains a severe issue and blocks the realization of complex problems with high speed and accuracy. Moreover, in extensively data-centric applications like artificial intelligence (AI), novel computational paradigms are vital to bring down power consumption. Neuromorphic computing based on resistive switching (RS) devices, or memristors, is a brain-inspired technology that has emerged as a viable ultra-low power consumption alternative. In this technology, information processing is performed directly at the memory element, preventing data shuffling and, therefore, enabling cost and power-efficient, real-time in-memory computation.

The memristor, discovered by Chua [1], is a non-linear resistor, usually composed of a metal-oxide-metal structure in which the metal layers compose the electrodes and an oxide film is referred to as active layer. Typically, these devices are fabricated in a vertical stack which allows for further miniaturization when compared with technologies such as Static random-access memory (SRAM), dynamic random-access memory (DRAM) or flash, as evidenced by the smallest 4 nm^2 device reported up to now [2]. The most interesting feature of the memristor is the fact that its resistance state can be tuned by an external electric field into two or more distinct states. The switching process occurs at the active layer and the transition from the highest-resistance state (HRS) to the lowest-resistance state (LRS) is known as set operation and from LRS to HRS, as reset operation. An exceedingly fast 50 ps switching speed has been obtained which is,

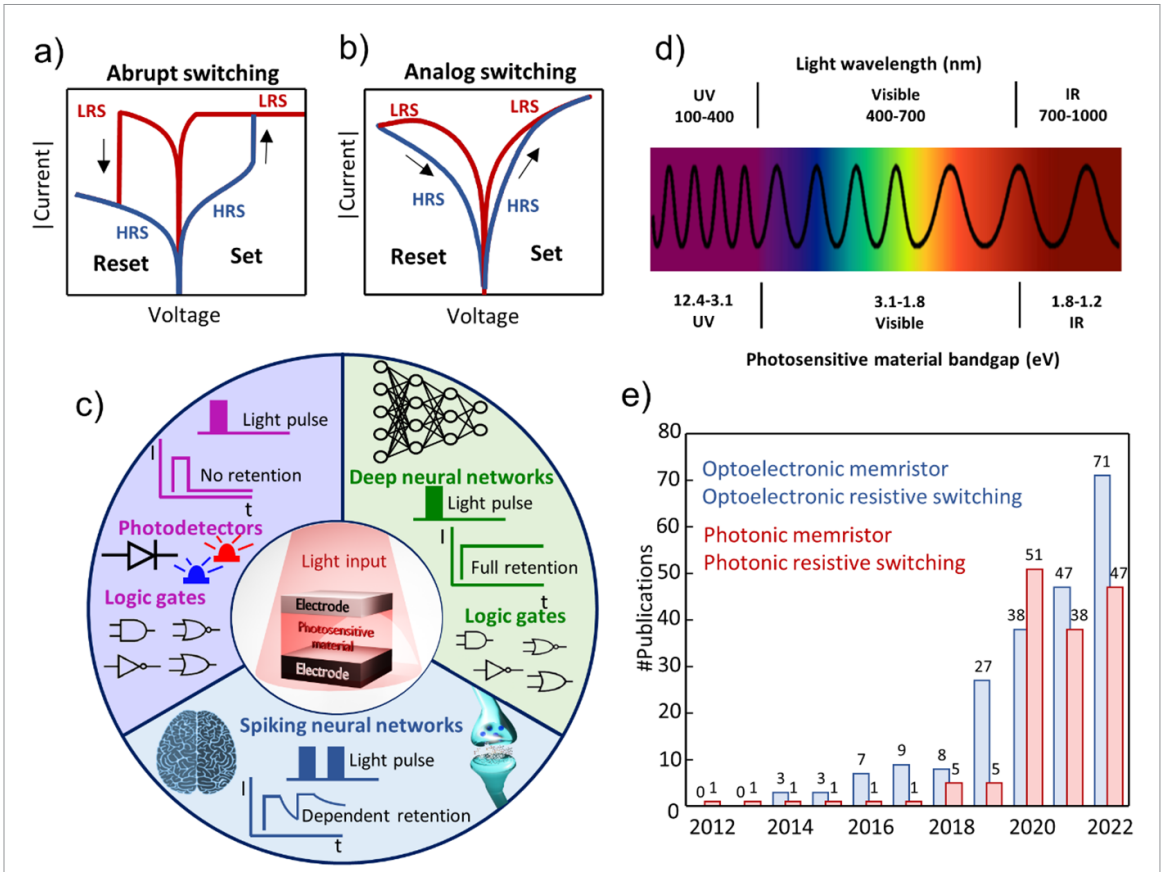

Figure 1. Typical memristor DC sweep showing (a) abrupt and (b) analog type of switching displaying set and reset for positive and negative polarities, respectively. (c) Illustration of potential OEMs applications and their state retention upon light pulse requirements. (d) UV-IR electromagnetic spectrum with light wavelength and bandgap material relation described. (e) Publications on optoelectronic and photonic memristors from 2012 to 2022 (search engine: Google Scholar, accessed on January 2023; keywords: optoelectronic memristor; optoelectronic RRAM; Photonic memristor; Photonic RRAM).

naturally, of extreme importance to ensure power efficiency [3, 4]. The retention of the programmed states is related to the material structure of the device and can be translated into short- or long-term memory behavior, suited for different neuromorphic applications.

The first fabricated memristor was reported in 2008 with TiO_2 as active layer and Pt as electrodes [5]. To date, the most popular materials for oxide-based memristive devices are still the transition metal oxides, for which the switching occurs, most commonly, in a filamentary form, such as tantalum oxide (Ta_2O_5), hafnium oxide (HfO_2) or aluminum oxide (Al_2O_3) [6–8]. Typically, the transition between different resistance states is an abrupt one, as exemplified in figure 1(a). An initial step, called electroforming, is required to create conductive filaments (CFs), usually composed of oxygen vacancies, within the insulating layer. This is, usually, accomplished with a once electric bias application of higher voltage than the operating one. Once these filaments are created, current can pass through which decreases the resistance of the device, now at the LRS. Then an operating voltage will cause the dissolution and consequent restoration of CFs resulting in set and reset operations. The CFs are typically robust and can only be dissolved by the operating voltage which results in long retention of programmed states. In the case of valence change memories, the dominant mechanism is determined by the balance between thermochemical and electrochemical redox reactions, which is mostly defined by the combination of the materials used in the device stack [9–11].

As opposed to abrupt-RS, analog switching behavior, displayed in figure 1(b), can be achieved using, for example, oxide semiconductors such as zinc oxide (ZnO), indium-gallium-zinc oxide (IGZO) or zinc-tin oxide (ZTO) as active layers [12–16]. Typically, this type of switching occurs at the interface and is attributed to an interchange or trapping of ions between a metal electrode and the oxide [17]. It, usually, results in a lower device-to-device (D2D) and cycle-to-cycle (C2C) variability, since an area-dependent behavior with a uniform contribution of defects is in place. Additionally, the programmed resistance state is, usually, not retained for a long period of time and is, instead, gradually replaced by the equilibrium state of the oxide. This retention time can be manipulated with the amplitude or number of programming electric pulses [18]. This behavior is unsuited for inference-only applications in which a stable retention of at least two well-separated states is required. However, it can be advantageous in the realization of synaptic functions.

Moreover, the manipulation of several distinct resistance states can be accomplished by both the abrupt and the analog RS and is preferred for in-memory computation tasks in stateful logic and/or artificial neural networks (ANN) loosely inspired by the human brain. An ANN hardware composed by interconnected and adaptive electronic elements was first envisioned in 1962 [19] and can be accomplished with RS devices organized in crossbars to perform parallel data processing. The human brain has 10^{11} neurons that communicate between each other through more than 10^{14} synapses, in which their connection strength varies [20]. In deep neural networks (DNNs) composed by memristor crossbars, synaptic behavior is mimicked when electric short pulses are continuously applied to the device to gradually decrease or increase its resistance state, in processes called potentiation and depression, respectively. In fact, several synaptic characteristics have already been emulated by RS devices [13, 21, 22] proving its overwhelming potential to substitute the classical computing system.

Nonetheless, memristor crossbars that operate under only electric stimuli often suffer from heat generation and crosstalk issues, related to the interference of neighboring devices, which is blocking high-scale implementation [23]. Crosstalk can be eliminated with the addition of a selector transistor in each crossbar cell. However, this approach undoubtedly increases cell area and energy consumption [24]. In fact, the biological system cannot be matched with purely voltage-assisted neuromorphic platforms. The human brain itself is stimulated by a number of sensing inputs such as light, sound, smells or touch, with about 80% of this information being acquired through visual perception [20]. Hence, an ideal AI system should merge the capabilities offered by electrical and optical domains [25].

Optoelectronic memristors (OEMs) use both light and electronic signals as inputs and can behave as sensory artificial synapses with high energy-efficiency, low crosstalk and fast data processing and are, thus, suitable to link artificial visual systems with its processing on hardware [26]. In detail, OEM technology offers the possibility of a non-electric programming method, and can, thus, be an enhanced solution to challenges such as excessive Joule heating and crosstalk that occur in high-density passive crossbar architectures. Beyond that, learning functions and signal transmissions cannot be simultaneously performed on devices operated solely with electric field. Adding light as a third terminal facilitates parallel data transmission and processing. Hence, the applications of such a system can be extended to all mobile computing applications where the near/in sensor computation concept is developed such as wearables, visual information processing, invisible touch screens, electronic eyes, and smart processors.

To build an OEM, firstly one must consider the targeted application, since a particular set of requirements related to its performance will be in place. Figure 1(c) illustrates the most relevant applications of reported OEMs in literature. As a photodetector, the optical induced change in resistance should only be detected during light input since the purpose is to reveal when there is, in fact, light irradiation. Contrary, in DNNs a quasi-full state retention after light pulse is mandatory for the highest accuracies in any task. In its turn, spiking neural networks (SNNs) is the paradigm closer to accurately simulating brain functionality and demands a dependent state retention on several factors such as number or frequency of applied input light pulses to mimic learning and forgetting capabilities of the human brain.

The retention of the light provoked resistance state is, usually, ascribed to a persistent photoconductivity (PPC) effect that is, often, inherent to the active layer material [27–30]. The PPC effect is, typically, attributed to (i) macroscopic physical barriers at the interfaces or doping defects that decrease the rate of recombination of photogenerated electron/hole pairs [31] or (ii) atomic scale barriers located at the large lattice relaxation sites in which the energy level of the empty defects is above the conduction band minimum and the occupied energy level is located in the band gap, preventing recombination [29, 32].

Consequently, the choice of memristor material structure is of the most importance. There should be at least one transparent electrode, such as indium-tin oxide (ITO) or aluminum-doped ZnO (AZO) [33–36], or a nm thick semi-transparent electrode, such Au, to allow light to reach the active layer. Moreover, the bandgap of the active layer material should be considered for proper light wavelength irradiation, as depicted in figure 1(d). Naturally, a lower bandgap material is desired for wide sensitivity to multiple wavelengths. However, these materials often suffer from inferior retention stability.

As evidenced in the graph of figure 1(e), where the number of publications in optoelectronic and photonic RS devices is presented pear year, there is an obvious growing interest in researching OEMs, as their potential becomes more and more clear. However, as it is still a novel topic, only few review articles can be efficiently consulted for a comprehensive analysis on the recent advances.

This review paper aims to fill in this gap, providing a summary on the developments on inorganic-based OEMs fabricated in a vertical stack, with focus on metal and semiconducting-oxides, 2D-based materials and 1D structures as active layer. The planar structure has also been widely explored [37–42], however for high-scale integration and power-efficiency, the vertical stack is the favored one. Organic materials have also been widely investigated for optoelectronic features [43–46] due to their advantages in low temperature and simple solution processing techniques. In addition, organic molecular tuning is possible and desirable which

leads to certain optical and electrical properties [47]. Nevertheless, organic materials are not, usually, as stable as inorganic ones mainly due to oxidation issues. In optoelectronic applications, metal oxide semiconductors are the ones which show high mobility and sufficient mechanical and electrical stability, besides transparency in some cases [48]. Furthermore, recent works of inorganic materials show immense progress in low-cost fabrication techniques using solution and printing methods [49]. Other classes of materials explored as active layer for optoelectronic features are ferroelectric or magnetic [50–53] and organic/inorganic perovskites materials [54–64]. However, most of the available studies are at the device level and, therefore, only a small sum have demonstrated synaptic functions [40, 65–67] or logic gates implementation [35, 68–71].

The potential applications of OEMs based on the targeted materials in logic gates, ANNs and, in more detail, on artificial visual systems are also evaluated here, with the assist of the reported individual features. Additionally, the current challenges and future perspectives in this field are also discussed.

2. OEMs: materials and devices

2.1. Metal oxide OEMs

The first report on controlling the resistance state in a memristor using light in combination with voltage signals was in 2012 by Ungureanu *et al* [72]. An active layer of Al_2O_3 on a Si/SiO_2 substrate was used with patterned Pd as top electrode. Under dark, there was barely any RS and the device could be considered a resistor, but combining −10/10 V electric pulses and a 6 V read pulse with ultraviolet (UV) or infrared (IR) light pulses, multiple resistance states could be achieved. As soon as light was switched off, the dark current value immediately returned, showing no PPC effect. However, for data storage and short/long-term memory applications, PPC effect is required. This long-lived effect after light exposure is beneficial to modulate a non-volatile multi-resistance state.

Later, HfO_x was proposed using Si substrates as bottom contact and Au [73] or Pt [74] as top electrodes. In these preliminary studies, PPC effect was not shown or discussed. In fact, the authors show RS behavior only under light irradiation. The former showed RS behavior under a broadband halogen–tungsten light source with multiple resistance states dependent on light intensity. The latter showed visible light sensitivity, with blue irradiation enabling RS characteristics. In this case, the optically boosted carriers transfer from Si together with electrically redistributed oxygen vacancies within the oxide, result in the switching behavior under light. Since these devices show memristive switching characteristics only under light, logic gates could be targeted as application, in which light is irradiated constantly from surroundings.

Light can be used as a third input to control set or reset operations in OEMs for a more power-efficient and fast approach. For instance, light irradiation was found to perform reset in a HfO_x-based memristor [75]. The proposed structure, illustrated in figure 2(a), presented a typical bipolar and abrupt switching behavior in dark, as shown in figure 2(b), with a high I_{LRS}/I_{HRS} ratio of more than 10^3. When the device was set in the LRS, visible light irradiation forced a transition to a higher resistance state and depending on its intensity, could perform a full reset. Figure 2(c) presents a graph where multiple resistance states can be distinguished that correspond to different light intensities for multilevel cell (MLC) operation. The different resistance states were proven to be non-volatile, which is related to the light-sensing mechanism. As explained before, this abrupt-type of switching is, usually, associated with the formation and rupture of CFs with different dimensions located within the oxide layer bandgap. A small CF is composed of a low amount of oxygen vacancies and, therefore, requires low light intensity for recombination with the surrounding oxygen interstitials, which causes filament rupture. A large CF is formed by a higher amount of oxygen vacancies and, thus, requires light of higher intensity to be annihilated. Additionally, it was observed that blue light triggers the same reset effect as white light while the longer, less energetic, wavelength of red light did not incite any reaction. The dependency on light wavelength was suggested to be associated with the position of oxygen vacancies inside the HfO_x bandgap after set. In fact, a wide-bandgap oxide such as HfO_x ($E_g = 5.7$ eV) is by nature not photo-responsive. However, photoexcitation of defects located at a level of ≈2–3 eV below the conduction band minimum is possible and would bring the device back to its initial HRS [75].

Similarly, More *et al* proposed a titanium oxide (TiO_x)-based memristor in which illumination with a tungsten lamp could decrease V_{Reset} from 3.5 V to 0.8 V, reducing energy consumption [76]. More recently, a $Pt/TiO_x/Ti$ memristor was reported to respond to multiple irradiation wavelengths, ranging from UV to red light, in a completely different manner [77]. In this work, an analog-type of switching was observed for $Pt/TiO_x/Ti$ devices. The current state increased as the irradiated wavelength shortened, particularly for blue and UV illumination, which is in agreement with TiO_x bandgap of ≈3.2 eV. Photons with shorter wavelengths provide enough energy to excite more electron–hole pairs within the TiO_x layer.

A different mechanism for photoexcitation was proposed by Zhou *et al*, related to a Pd/molybdenum oxide (MoO_x)/ITO memristor structure [78]. In this study, a light induced manipulation of Mo valence

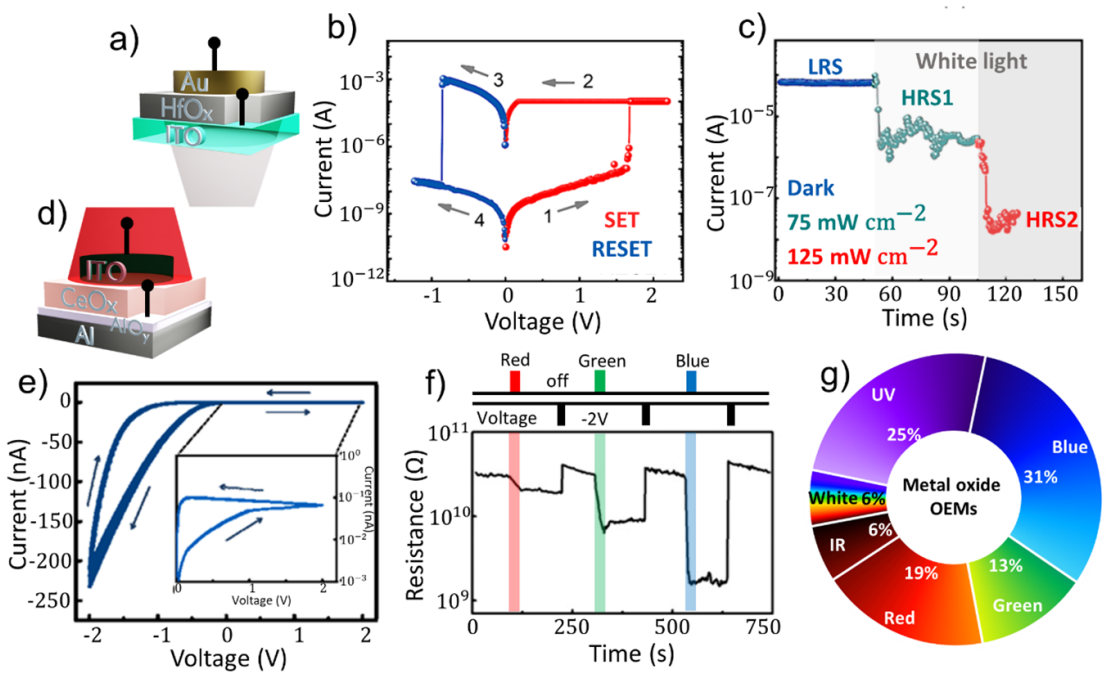

Figure 2. Metal oxide OEM characteristics. (a) ITO/HfO_x/Au OEM illustrative structure; (b) correspondent abrupt behavior in IV sweep displaying set/reset for positive/negative polarities, respectively and (c) correspondent LRS read at 0.1 V in the dark, during 75 mW cm^{-2} and 125 mW cm^{-2} of white light irradiation. Reprinted (adapted) with permission from [75]. Copyright (2019) American Chemical Society. (d) Al/Al_2O_3/CeO_x/ITO illustrative structure; (e) correspondent analog behavior in IV sweep displaying set/reset for positive/negative polarities, respectively and (f) resistance state measured in time with alternative dark and light irradiation (red/green/blue cycles) with reset electrical pulse of −2 V before each cycle. [80] John Wiley & Sons. [© 2015 WILEY-VCH Verlag GmbH & Co. KGaA, Weinheim]. (g) Statistical percentage on the light wavelength inducing RS reported by the works on metal oxide-based vertical OEMs.

states in the MoO_x thin film explained the photonic set. UV light irradiation caused the generation of electrons and holes in the MoO_x layer. As photogenerated electrons transferred to the MoO_x conduction band, a reaction would take place between photogenerated holes and absorbed water molecules that produced protons (H^+). Under surface science studies, authors revealed that the photogenerated electrons together with the protons would trigger the creation of H_yMoO_x and incite a shift from Mo^{6+} to Mo^{5+}, which ultimately resulted in the increase of current to LRS. When light was switched off, the current state did not return to HRS and, instead, suffered a slow decay (PPC effect). During electronic reset, an electric field forced the protons away from the MoO_x layer towards the Pd electrode and Mo^{5+} changed back to Mo^{6+}, causing a decrease in current state to HRS.

A bi-layer structure of Ta_2O_{5-x}/Ta_2O_5, sandwiched between an Si substrate and an Ag top electrode, demonstrated significant potential as an OEM [79]. This device showed a dependent current increase on UV and visible light irradiation with full retention of the photo-produced states, proving light information can be stored *in situ*. The bandgap of Ta_2O_5 is ≈4.0 eV, and therefore, it responds mostly to UV light. However, due to oxygen vacancies in the Ta_2O_{5-x} film, the electrons at the defect energy level can still be forced to the conduction band by lower energy wavelengths.

Therefore, a bi-layer switching medium can be used to enhance the performance of optoelectronic features, similar to electric field-induced counterpart. The AlO_y/Cerium oxide (CeO_x) memristor with Al as bottom and ITO as top contacts- figure 2(d)- was reported by Tan *et al* [80–82]. A native AlO_y layer was created upon deposition of Al to form the Schottky junction with the CeO_x, that resulted in analog switching behavior, shown in figure 2(e). The photo-sensitive mechanism was explained by electrons trapped in the oxygen vacancies at the AlO_y/CeO_x interface. These electrons could be excited by photons and leave positively charged oxygen vacancies. This would lower the effective Schottky barrier by reducing its width, which would cause a decrease in the resistance of the junction. This memristor structure presented photocurrents dependent both on light intensity and wavelength, as shown in figure 2(f). Naturally, shorter wavelengths and higher light intensity triggered the highest current change. Moreover, PPC effect could be noticed as, even after light pulse, the current state remained unaltered. A voltage reset was then required to fully erase the resistance state.

Additionally, metal-oxide materials have been used in double-layer strategies in combination with semiconducting-oxides for switching medium in OEMs and will be discussed in the following section. In

table 1, the comparison of the most important characteristics in metal-oxide OEMs can be consulted and it is noticeable some devices show optical set/reset coupled with electric reset/set, respectively. Naturally, photo-induced switching can be abrupt or analog depending on material stacks. The working principal of analog optical memristors is mainly related to the change of barrier profile at the interface of the electrode and the switching layer, which resembles to analog electric field-induced RS devices. Abrupt optical RS shows higher retention stability, however, inferior C2C and D2D reproducibility is expected due to the switching dependent on CFs. When reset is induced by light, the resistance state obtained is always maintained after light pulse. However, this is not considered PPC since, in this case, light is used to partially/fully break CFs and not to increase the conductance state.

No fully photonic switching behavior has been demonstrated within the same device, which hinders their possible application in wire-free crossbars. Moreover, as demonstrated in figure 2(g), most studies report on UV or blue irradiation which makes the discrimination between signals of different wavelengths challenging. Future technology will rely on visible light communication, where the application of abundant light sourcing devices (lamps, mobile displays, TV, etc) will be very important in the concept of ambient intelligence.

2.2. Oxide semiconductors OEMs

Oxide semiconductors can provide additional advantages as active layer on memristors. In particular, amorphous oxide semiconductors (AOS), such as IGZO or ZTO, have high flexibility, due to a lack of grain boundaries, which enables low-processing temperatures. This facilitates the use of flexible substrates (paper, polyimide, polyethylene naphthalate (poly(ethylene 2,6-naphthalate) (PEN) / polyethylene terephthalate (PET) [24, 83, 84], providing the means for embedded flexible technologies in wearables and internet-of-things applications. Furthermore, AOS are used in flat-panel display technology for active-matrix driver circuits, making them ideal candidates for future integrated memristor-based hardware for AI.

ZnO has been the most popular material as switching medium for OE devices. Using Pt and ITO as bottom and top contacts, Xie *et al* showed a decrease in V_{Set} and V_{Reset} upon UV light for more efficient power consumption [85]. Contrary, Shih *et al* showed an increase in V_{Set} and V_{Reset} which is not very appealing [86]. However, PPC effect was present in these devices, as a change in RS behavior was observed even after UV light was turned off, which means ANNs could be targeted as applications. Moreover, the memristor showed improved I_{LRS}/I_{HRS} ratio after UV illumination. The authors explained that the conduction mechanism changed from Schottky emission to Poole–Frenkel after UV illumination, which induced the creation of extra oxygen ions and radicals due to an accelerated breaking of Zn–O bonds.

The analog behavior of the ZnO memristor was also studied using different electrodes for OE applications [87, 88]. UV light was proven to increase the current state with a PPC effect. Interestedly, one of the reported OE structures for analog-type of switching, ITO/ZnO/Ag [88], was also described by another group yet with an abrupt-type of RS [89]. On both reports, the sputtering technique is employed to deposit ZnO and similar thicknesses for all composing memristor layers are used. However, ZnO deposition conditions are different which can explain the observed results. Generally, electrochemical mechanism (ECM) is responsible for the RS in devices with active electrodes such as Ag and Cu. In this respect, depending on the electric field, switching can be tuned to be abrupt for higher field or analog, depending on the size of metallic filament. The analog RS behavior could be also related to interface properties of ZnO with the contacts which is directly related to deposition conditions. In fact, in the original works, the reported analog switching for this memristor structure is associated with oxygen vacancies filaments whereas the abrupt switching is related to ECM with Ag filaments [88, 89].

A semi-transparent ZnO OEM, with Pt and Au as electrodes, that could perform both set and reset with optical inputs has been developed, with the structure illustrated in figure 3(a) [90]. In detail, Yang and co-workers showed set could be induced by UV, blue or green irradiation with PPC characteristics, showing MLC operation. UV illumination resulted in the highest current increase with an I_{LRS}/I_{HRS} ratio of $\approx 10^4$. Nonetheless, less energetic wavelengths such as green light could also induce a sufficiently high I_{LRS}/I_{HRS} ratio of $\approx 10^2$, as can be seen in figure 3(b). ZnO has a wide bandgap of 3.2 eV. However, deposition in pure Ar atmosphere can result in a larger amount of oxygen vacancies along with material heterogeneity with different energy levels [91]. Visible light irradiation can, thus, induce an ionization of oxygen vacancies, converting them into positively charged oxygen vacancies and free electrons which leads to an increase of the current state, as commonly accepted for AOS materials [92]. Interestingly, the retention time (or PPC effect) was also impacted by light exposure. The retention decay was fastened by irradiation with longer wavelengths such as red and near-IR (NIR) illumination, leading to an optical reset, in the scale of seconds (see figure 3(b)). This photonic reset was explained with an injection of electrons from the metal to the ZnO layer, by internal photoemission or photo-assisted tunneling. Part of these electrons neutralized ionized oxygen vacancies, decreasing its density, and fastening the PPC decay.

Table 1. Characteristics of vertical OEMs with metal oxides as active layer. N.S.: not specified at the original paper; N.A.: not applicable; BB: broadband. Endurance is related to optical induced RS properties.

Active layer	Electrodes	Size (μm^2)	RS behavior	λ_{light} (nm)	Light effect	DC sweep set/reset (V)	I_{LRS}/I_{HRS} ratio	Endurance (cycles)	Electric retention	PPC	References
Al_2O_3	Si/Pd	1.00×10^8	Abrupt	390 950	Enables switching behavior	−10/10	$>1.00 \times 10^3$	N.S.	1 year	No	[72]
HfO_x	Si/Au	4.00×10^4	Abrupt	BB	Enables switching behavior	4.0/−4.0	$>1.00 \times 10^3$	N.S.	N.S.	N.S.	[73]
HfO_x	p-Si/Pt	1.26×10^3	Abrupt	450	Enables switching behavior	6.0/−4.0	$\approx 1.00 \times 10^4$	N.S.	1.00×10^4	N.S.	[74]
HfO_x	ITO/Au	N.S.	Abrupt	400 400–700	Performs reset	2.6/−1.2	$>1.00 \times 10^3$	25	1.00×10^3	N.A.	[75]
TiO_x	Al/Pt	5.00×10^1	Abrupt	320–1100	Decreases V_{Reset}	5.0/5.0	$>1.00 \times 10^1$	300	6.00×10^5	N.A.	[76]
TiO_x	Pt/Ti	4.91×10^2	Analog	365 465 532 650	Increases current	3.0/−3.0	N.S.	N.S.	No	Yes	[77]
MoO_x	ITO/Pd	4.91×10^4	Abrupt	365	Performs set	N.S./−2.5	$\approx 4.00 \times 10^1$	N.S.	1.44×10^3	Yes	[78]
Ta_2O_{5-x}/Ta_2O_5	N-Si/Ag	1.26×10^3	Abrupt	460 620	Performs set	4.0/−4.0	$\approx 3.00 \times 10^3$	10	2.00×10^4	Yes	[79]
AlO_y/CeO_{2-x}	Al/ITO	7.85×10^3	Analog	254 499 560 638	Performs set	2.0/−2.0	$\approx 1.00 \times 10^3$	30	1.00×10^4	Yes	[80, 81]

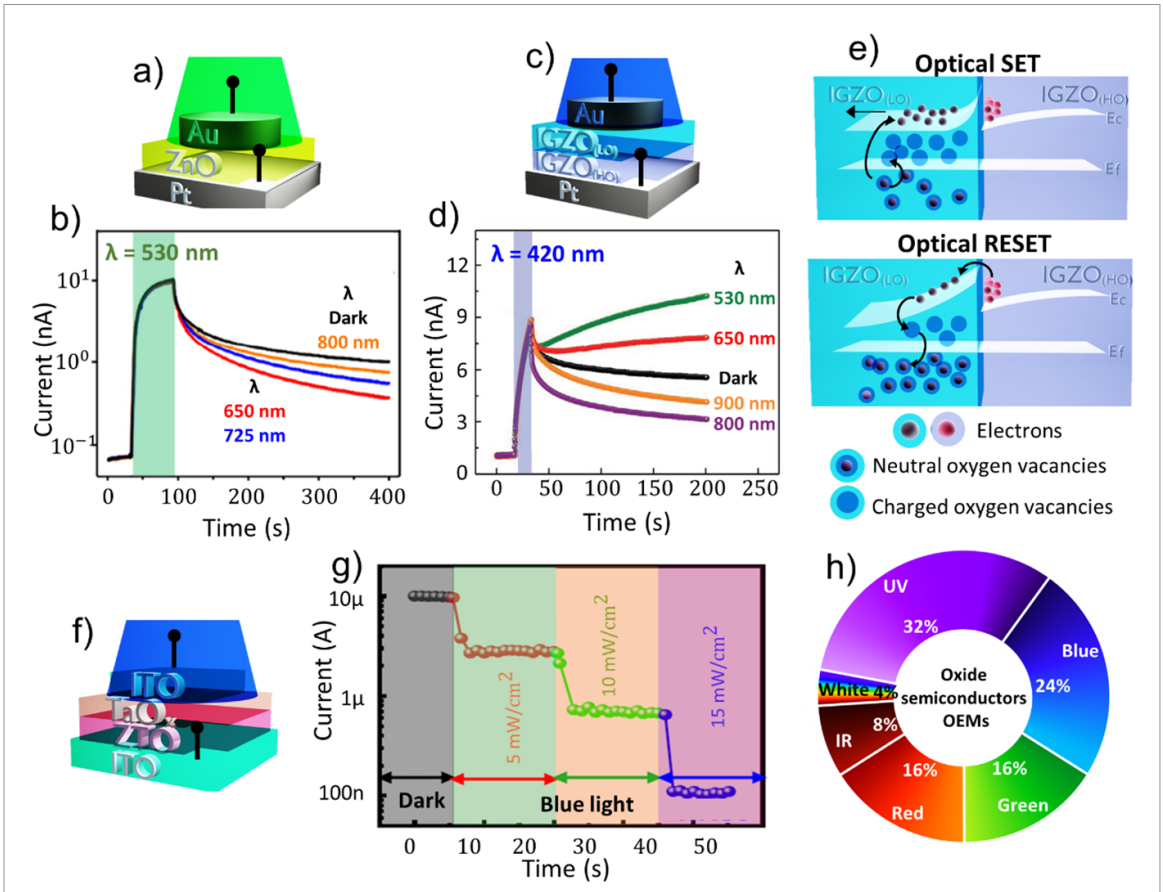

Figure 3. Oxide semiconductors OEMs characteristic behaviors. (a) Pt/ZnO/Au OEM illustrative structure and (b) correspondent current increase under green light irradiation and PPC decay fastened by 650, 725 and 800 nm wavelength of light. Reproduced from [90]. CC BY 4.0. (c) Pt/$IGZO_{(HO)}$/$IGZO_{(LO)}$/Au OEM illustrative structure and (d) correspondent current increase under blue light irradiation and PPC decay fastened by 800 and 900 nm wavelength of light. (e) Schematic illustrations of oxygen vacancies ionization and neutralization during light irradiation on optical set and reset operations. The reaction marked by arrows plays a dominating role in the OE response. Reproduced from [26]. CC BY 4.0. (f) ITO/ZTO/TaO_x/ITO OEM illustrative structure and (g) correspondent multilevel states achieved by different blue light intensities. Reprinted (adapted) with permission from [97]. Copyright (2022) American Chemical Society. (h) Statistical percentage on the light wavelength inducing RS reported by the works on oxide semiconductors OEMs.

Similarly, the same research group showed photonic set and reset in a double layer IGZO memristor, illustrated in figure 3(c) [26]. The analog RS behavior was attributed to the formation of a potential barrier and well at the interface of a layer with low oxygen (LO) content ($IGZO_{(LO)}$) and a layer with high oxygen (HO) content ($IGZO_{(HO)}$). The width of this interfacial barrier would be dependent on the ionized oxygen vacancies density. The lower this density, the smaller the barrier, which facilitates electron tunneling and increases the current state of the device. On the other hand, during reset, the neutralization of ionized oxygen vacancies would increase the barrier width and result in a decrease of current state. Set could be induced by light in wavelengths from 420 to 1000 nm. Naturally, the longer the wavelength used for irradiation, the less change the current state would suffer. It was found that the PPC decay time could be decreased (reset) by red or NIR (800/900 nm) light, only if the previous set process was performed by short wavelengths illumination (350/420 nm), as can be seen in figure 3(d). To explain this phenomenon, the authors proposed that during illumination, the photocurrent would depend on a dynamic equilibrium between ionization and neutralization of oxygen vacancies (figure 3(e)). When the memristor was exposed to visible light of higher energy to perform set, a small amount of oxygen vacancies was left that could be further ionized by subsequent irradiation with light of lower energy. In this case, a neutralization of oxygen vacancies would, therefore, be dominant and enable a decrease in the current state-reset.

Later, a double-layer ZTO OEM was described, following the above explained strategy of oxygen rich and deficient layers [93]. Set was performed electrically with $a \approx 10^2$ I_{LRS}/I_{HRS} ratio. Reset could be performed with MLC properties via blue, green and red light irradiation and the I_{HRS} was not only dependent on wavelength, but also on light power. It was clarified that light would provide the necessary energy for interstitial ions to recombine with electrically produced oxygen vacancies within the ZTO layer, causing CFs to disrupt. Interestedly, analyzing the DC sweep displaying RS behavior, set and reset transitions do not seem abrupt. However, the CF formation/annihilation explanation for the RS behavior is aligned with the full 10^5 s retention of states obtained for this memristor structure. The same behavior was observed in a bilayer

memristor with ZTO/TaO_x (structure illustrated in figure 3(f)), in which MLC could be achieved by different power of blue light irradiation, as can be seen in figure 3(g).

In table 2, a list is provided with the most relevant features on the, so far reported, OEMs based on oxide semiconductor materials and bi-layers. To our knowledge, this class of materials was the only one so far not relying on nanostructured materials to demonstrate full photonic RS behavior with set and reset being performed by light with different wavelengths. However, as evidenced by the statistical percentages on different light-induced RS presented in figure 3(h), the research is, still, mostly on UV and blue light irradiation. Since IR light is the transmission method for data in wireless systems, it is highly desirable that further research on longer wavelengths is realized to allow conversion and storage of IR data [94]. High-speed process is one of the main challenges for further development of OEMs, relying on the working principal as mentioned in most of the reports. In this respect, there are several solutions such as increase the built-in potential by engineering the memristive device layer stack, either via defect engineering of the RS layers or via modification of the effective work function at the contacts. The second main challenge is the bandgap tunability of oxide thin films for a broader spectrum. Here, the same approaches reported for visible light AOS-based photodetectors can be adopted. For instance, an absorption layer composed of hydrogen-doped IGZO revealed visible light detection [95]. RGB-color detection is also possible with strategies such as using a system combining an AOS film with colloidal quantum dots (QDs) [96], as will be later discussed.

2.3. 2D-materials OEMs

Two-dimensional-materials such as graphene (G), transition metal dichalcogenides (MoS_2, WS_2, WSe_2, $MoSe_2$, $MoTe_2$, etc) or black phosphorus (BP), have also been widely explored for OEMs due their excellent photoresponsivity [104], related to a large surface-to-volume ratio, and RS switching performance [105, 106]. A review paper from 2019 can be consulted, where mainly planar 2D-based structures for OEMs are described in detail, to that date [94]. Here, as previously explained, the focus is on vertically stacked devices, which were mostly reported more recently.

In this regard, a monolayer of MoS_2 was used as switching medium in Si substrates and W top electrodes [30]. UV illumination was used to perform set with one order of magnitude of I_{LRS}/I_{HRS} ratio and PPC effect was observed related to a spontaneous trapping/detrapping of electrons. However, the necessary voltage to perform reset on these devices was high (-8 V). Since this monolayer has a bandgap of 1.8 eV, it would be interesting to test these devices under IR illumination. In another study, WO_3 OEMs showed enhanced performance under light input [107]. A combination of a 600 °C annealing and 45 min of white light irradiation resulted in an improved I_{LRS}/I_{HRS} ratio that went from 1.7 (as-prepared device) to 25.

Later, Jaafar and Kemp demonstrated a current increase induced by UV light in a GO based-memristor [108]. Here, a planar structure was compared to a vertical one. The latter showed superior features with an abrupt RS of $\approx 10^4$ ratio. Moreover, during UV irradiation, both V_{Set} and V_{Reset} were reduced. This behavior was attributed to photogenerated electron–hole pairs which increased the current state in both LRS and HRS. A PPC decay was also shown, that can be useful for ANNs applications.

Reset induced by light was also reported on 2D OEMs. For instance, an heterostructure of $MoSe_2/Bi_2Se_3$ nanosheets was embedded in a polymethyl methacrylate (PMMA) film to form the active layer on a device that showed reset under NIR light [109]. PMMA was included in the active layer to passivate the trap states on $MoSe_2/Bi_2Se_3$. The full device structure is illustrated in figure 4(a). The memristor showed abrupt RS behavior assigned to Joule-heating provoked formation/disruption of metallic CFs. The authors explained NIR light would facilitate the rupture and prevent the creation of CFs since the Ag clusters would react with photogenerated holes and oxidize back to Ag^+. In the graph of figure 4(b), the current state of the device with multiple stimulus can be evaluated in time. It can be seen that the current decreases to the full-HRS only under both NIR illumination and electric reset.

A different mechanism for reset by light was proposed by Zhou *et al* regarding a memristor based on BP nanosheets coated with polystyrene (PS) (BP@PS) [110], with the structure illustrated in figure 4(c). The DC sweep displaying set and reset under different light wavelengths can be consulted in figure 4(d). It is clear that a higher energy illumination, further decreased V_{Reset} from 2 V (dark) to 1.17 V (UV), as summarily presented in figure 4(e), and achieved a lower current state in the HRS, enabling higher I_{LRS}/I_{HRS} ratio. The authors explained that during electric reset, the external electric field would change the direction of the internal electrical field (induced by a transfer of electrons from the BP@PS to the ITO layer, due to the different material work functions), forming a Schottky barrier. When the memristor was exposed to light, the trapping sites would capture the photogenerated electrons and the surface potential would increase, further increasing the Schottky barrier, and, therefore, increasing I_{LRS}/I_{HRS} ratio. Additionally, as the scattering centers were negatively charged by the captured photogenerated electrons, the internal electric field would increase and a lower V_{Reset} would be necessary to switch off the device.

Table 2. Characteristics of vertical OEMs based on semiconductor oxides and bilayer structures composed of metal/semiconducting oxides as active layer. N.S.: not specified at the original paper; N.A.: not applicable. Endurance is related to optical induced RS properties.

Active layer	Electrodes	Size (μm^2)	RS behavior	λ_{light} (nm)	Light effect	DC Sweep Set/Reset (V)	I_{LRS}/I_{HRS} ratio	Endurance (cycles)	Electric retention	PPC	References
ZnO	Pt/Pt	3.14×10^4	Abrupt	365	Adds intermediate state	2.2/1.1	$\approx 1.00 \times 10^2$	100	N.S.	No	[98]
ZnO	Pt/ITO	1.96×10^5	Abrupt	365	Decreases V_{Set}/V_{Reset} Adds intermediate state	2.0/−2.0	$\approx 4.00 \times 10^1$	N.S.	1.00×10^4	N.S.	[85]
ZnO	TiN/ITO	$4.00 \times 10^{\circ}$	Abrupt	<380	Increases V_{Set}/V_{Reset} Decreases I_{HRS}	−0.1/0.3	$\approx 1.00 \times 10^1$	N.S.	N.S.	N.A.	[86]
ZnO	FTO/In_2O_3	N.S.	Analog	365	Increases current	2.0/−2.0	N.S.	N.S.	N.S.	Yes	[87]
ZnO	ITO/Ag	7.85×10^3	Analog	366	Increases current	1.5/−1.5	N.S.	100	No	Yes	[88]
ZnO	Pt/Au	7.85×10^3	Analog	350 420 530 650 725 800	UV/Blue/Green performs set Red/IR performs reset	Nonpolar (−2.0/2.0)	$<1.00 \times 10^1$	20	N.S.	Yes	[90]
ZnO	ITO/Ag	4.00×10^4	Abrupt	White	Performs set	3.0/−3.0	$\approx 1.00 \times 10^1$	N.S.	1.00×10^4	Yes	[89]
$IGZO_{(HO)}$/ $IGZO_{(LO)}$	Pt/Au	7.85×10^3	Analog	420 530 650 800 900	VIS performs set IR performs reset	2.0/−2.0	$>1.00 \times 10^1$	10	1.00×10^4	Yes	[26]
ZTO_y/ZTO_x	ITO/ITO	1.00×10^4	Abrupt	450–495 495–570 620–760	Performs reset	1.0/−1.0	$\approx 1.00 \times 10^2$	2200 1800 1800	1.00×10^5	N.A.	[93]

(Continued.)

Table 2. (Continued.)

Active layer	Electrodes	Size (μm^2)	RS behavior	λ_{light} (nm)	Light effect	DC Sweep Set/Reset (V)	I_{LRS}/I_{HRS} ratio	Endurance (cycles)	Electric retention	PPC	References
ZTO/TaO_x	ITO/ITO	1.00×10^4	Analog	405	Performs reset	2.0/−2.5	$<1.00 \times 10^2$	1500	1.00×10^4	N.A.	[97]
ZTO	ITO/ITO	1.77×10^4	Analog	405	Increases current	2.0/−2.0	1.80×10^1	N.S.	1.00×10^4	Yes	[99]
SiO_x	p-Si/ITO	2.5×10^5	Abrupt	410 532 632 650	Increases I_{LRS} Decreases V_{Set}	6.0/−5.0	$\approx 1.00 \times 10^3$	N.S.	N.S.	Yes	[100]
AlO_y/ZnO_{1-x}	Al/ITO	7.85×10^3	Analog	310	Performs set Increases I_{LRS}	3.5/−6.5	$>1.00 \times 10^1$	N.S.	1.00×10^3 LRS	Yes	[101]
ZnO/CeO_x	ITO/TiN	3.14×10^4	Analog	405	Performs set	8.0/−8.0	$\approx 1.00 \times 10^1$	N.S.	N.S.	Yes	[102]
Al_2O_3/IGZO	Al/ITO	2.25×10^4	Analog	400	Enables switching behavior	3.0/−3.0	$8.00 \times 10^{\circ}$	N.S.	No	Yes	[103]

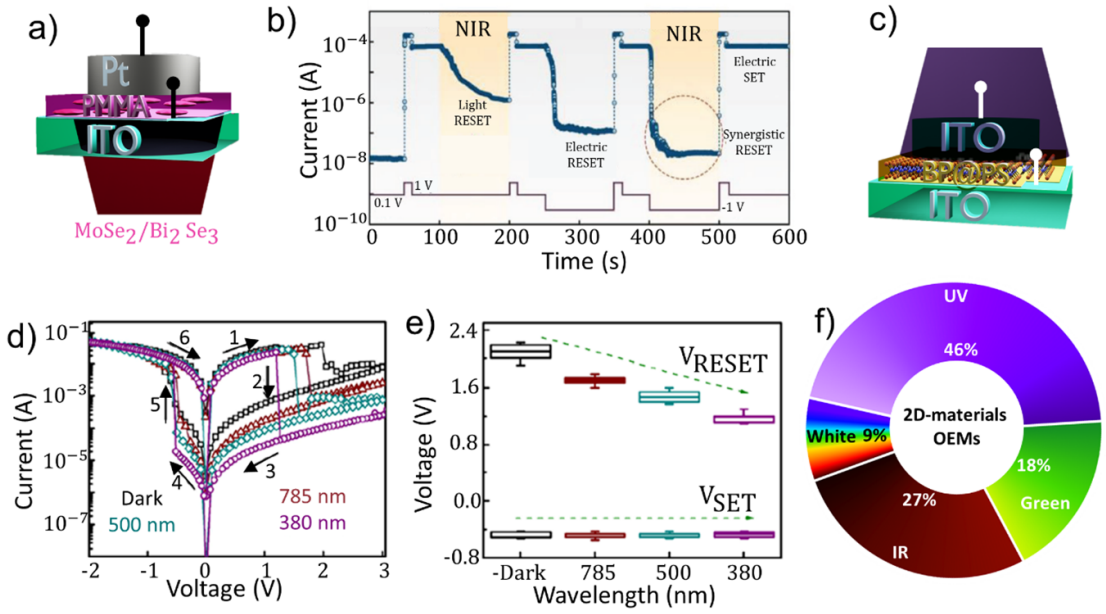

Figure 4. 2D-materials based OEMs characteristic behaviors. (a) ITO/$MoSe_2$/Bi_2Se_3@PMMA/Pt OEM illustrative structure and correspondent (b) current increase due to set electric pulse and induced current decrease due to IR light irradiation (1.65 mW cm^{-2}). A synergistic reset strategy, in which both electric and optical pulses are applied, could realize full reset. [109] John Wiley & Sons. [© 2019 WILEY-VCH Verlag GmbH & Co. KGaA, Weinheim]. (c) ITO/BP@PS/ITO OEM illustrative structure and correspondent (d) $I-V$ sweeps modulated by different wavelengths, displaying set/reset for negative/positive polarities, respectively and (e) V_{Set} and V_{Reset} obtained under different light illuminations. UV irradiation enables a smaller V_{Reset}. Reprinted (adapted) with permission from [110]. Copyright (2020) American Chemical Society. (f) Statistical percentage on the light wavelength inducing RS reported by the works on 2D-materials OEMs.

The research on 2D-materials for vertically stacked OEMs is still at its infancy and requires further investigation. A complete review on 2D-based memristors and its challenges and future perspectives can be consulted in [111], in which the need for the development of proper 2D material films, that can be employed in high performance devices in a large-scale, is emphasized. Once this is accomplished, it is expected that this type of OEMs will offer a faster and more energy efficient switching, due to the atomically thin characteristics of 2D materials [112]. In fact, the switching speed is not yet widely investigated in the small amount of available literature on vertically stacked OEMs based on 2D materials. As can be seen in table 3, so far, mostly abrupt RS related to trapping and detrapping of electrons was described, which is more advantageous for in-memory computation and DNNs applications. NIR light irradiation has been explored in a higher percentage when compared with other classes of materials, as evidenced by figure 4(f), mostly for reset operation. In fact, it has been previously observed that 2D-based photodetectors can be built for Terahertz detection [113, 114] which can be very promising for memristors. To our knowledge, no fully-photonic 2D-based memristor has been proposed.

2.4. 1D-structured OEMs

Another strategy to build an OEM is to take advantage of 1D structured materials, such as NRs or NPs (figure 5(a)), in order to achieve enhanced performance. Compared with thin-films, nanostructures provide higher surface-to-volume ratio and larger photon harvesting, that ultimately results in improved photoconductivity, with highly localized RS [117]. Another major advantage is the potential for miniaturization, as these nanostructures can usually be produced by bottom-up approaches allowing for a rigorous control of structures dimensions [118, 119].

The first report on a 1D-structured OEM dates back to 2012. Park *et al* reported on a ZnO NR-based device with FTO and Au as electrodes [120]. Showing an abrupt-behavior, RS was only observed when the device was illuminated by a xenon light source and was ascribed to oxygen vacancies filament formation/rupture. In the dark, oxygen molecules would be chemisorbed onto the surface of ZnO NRs acting as an oxygen source and preventing the oxygen vacancies filament formation. Upon light irradiation, electron–hole pairs would be created, and the holes would combine with oxygen ions adsorbed at the ZnO, allowing for CFs creation. Moreover, the modulation of light incident angle was shown to regulate RS in ZnO NRs [121]. In this work, a surface treatment was carried out to induce hydrophobic properties on ZnO NRs, inducing the formation of an air bubble protecting the memristor when emerged into water. The device

Table 3. Characteristics of vertical OEMs based on 2D-materials. N.S.: not specified at the original paper; N.A.: not applicable. Endurance is related to optical induced RS properties.

Active layer	Electrodes	Size (μm^2)	RS behavior	λ_{light} (nm)	Light effect	DC Sweep Set/Reset (V)	I_{LRS}/I_{HRS} ratio	Endurance (cycles)	Electric retention	PPC	References
MoS_2	p-Si/W	1.96×10^3	Analog	310	Performs set	7/−26	$>1.00 \times 10^1$	N.S.	No	Yes	[30]
WO_3	AZO/ITO	2.50×10^5	Abrupt	400–760	Enables RS behavior	6/−6	$\approx 2.00 \times 10^1$	200	1.00×10^3	Yes	[107]
GO	ITO/Ag	1.26×10^5	Abrupt	380	Increases current	1/−1	$\approx 1.00 \times 10^4$	5	N.S.	Yes	[108]
TiS_3	ITO/Al	3.14×10^4	Abrupt	400 530 808	Increases current	−1/2	$\approx 4.00 \times 10^2$	N.S.	1.00×10^4	N.S.	[115]
TiN_xO_{2-x}/MoS_2	ITO/Al	7.85×10^3	Analog	365	Increases current	3/−3	$\approx 1.00 \times 10^1$	N.S.	No	Yes	[116]
$MoSe_2/Bi_2Se_3$/PMMA	ITO/Ag	N.S.	Abrupt	790	Performs reset	2/−2	2.83×10^3	N.S.	1.00×10^6	N.A.	[109]
BP@PS	ITO/ITO	3.14×10^4	Abrupt	380 500 785	Performs reset	3/−1	1.52×10^3	N.S.	1.00×10^4	N.A.	[110]

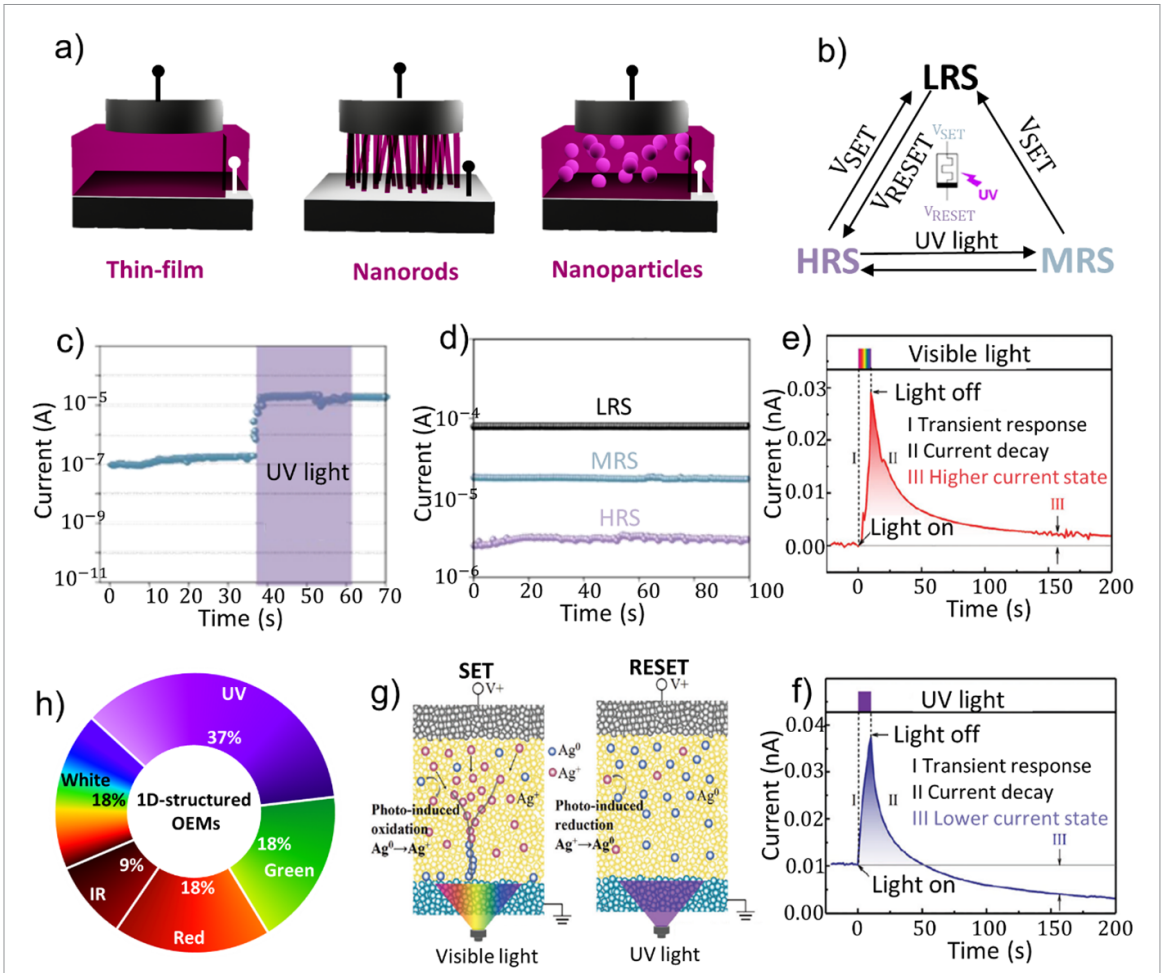

Figure 5. One-dimensional-structured OEMs characteristic behaviors. (a) Schematic illustration of memristors based on thin-films, NRs and NPs; (b) Proposed operating procedure using light as input to add an medium resistance state (MRS), on a memristor composed of Ag NPs embedded in Mxene-TiO_2 nanosheets and correspondent (c) current response under UV irradiation and (d) retention of the 3 resistance states achieved with this memristor structure. Reprinted (adapted) with permission from [126]. Copyright (2021) American Chemical Society. (e) Current increase under visible light irradiation (21.8 mW cm^{-2}) on a memristor based on Ag NPs embedded on a TiO_2 thin film. Once the light was turned off, the current decreased and stabilized in a state higher than the initial one (set) and (f) current response, correspondent to the same memristor structure, under UV illumination (3.7 mW cm^{-2}). When the light was turned off, the current decreased and stabilized in a state lower than the initial one (reset) and (g) correspondent proposed physical mechanism of light induced set and reset operations schematic illustrated. Reproduced from [127]. CC BY 4.0. (h) Statistical percentage on the light wavelength inducing RS reported by the works on 1D-structured based OEMs.

behaved as a resistor with no RS properties when the light beam incidence surpassed a critical angle at the water/air interface, because total internal reflection would occur and light would not reach the ZnO NRs. When the light beam incidence was below the critical angle, RS was observed. In another study, the photoconductivity of a ZnO NRs-based device was calculated to be about 10^4 and compared to the much lower 70 achieved in a ZTO thin-film based memristor [122].

Furthermore, an heterojunction composed of ZnO and phosphorene (ZP) NPs showed a decreased V_{Set} under irradiation of UV, green, red and IR light, with the possibility of MLC [123]. In another work, ZP NPs were sandwiched between two PMMA layers and an analog RS was observed [124], in which the current state could be increased by UV, green and red light. However, no PPC effect could be noticed.

Li *et al* proposed an heterostructure composed of PbS QDs crammed between ZnO thin-films [20]. The authors were able to design a photonic memristor making use on the bandgap of the ZnO film (3.37 eV) and of the PbS QDs (1.15 eV). An optical induced set was demonstrated by UV light, whereas photonic reset was performed by IR light. Upon UV light exposure the same explanation in the concept of ionized oxygen vacancies was given by authors. However, for lower light energies such as IR light irradiation, electrons from QDs are excited, neutralizing ionized oxygen vacancies, resulting in the decrease of the current state of the device.

Red light was used to achieve multiple states for MLC characteristics in a memristor composed of Sb_2Se_3/CdS NRs, with PPC effect [125]. The RS behavior was attributed to the formation/rupture of CFs. It

was clarified that under exposure, part of the irradiated light would be directly absorbed by NRs and other part would be reflected towards adjacent NRs, enhancing energy harvesting. NRs would act as trapping sites for photogenerated holes on the Se_2Sb_3 surface, which would increase the current state and the lifetime of photogenerated electrons, resulting in PPC effect.

Another interesting approach for MLC operation was proposed by Guo *et al.* The memristor structure, had an active layer composed of Ag NPs embedded in Mxene-TiO_2 nanosheets. In this study, both set and reset were accomplished by electrical means and an additional state, medium resistance state (MRS) was realized by exposure to UV light, as exemplified in figure 5(b). MRS could be 2 orders of magnitude higher than HRS with fair retention of states (figures 5(c) and (d)) [126]. The physical mechanism of switching was explained by oxygen vacancies CFs facilitated by Ag NPs. A missing peak of atom signals around Ag NPs was found on the TEM analysis, which the authors related to an oxygen vacancy where the conductive path on LRS would originate. UV light could create electron–hole pairs in the TiO_2, increasing the content of Ti^{3+} and, thus, facilitating the creation of oxygen vacancies. Therefore, Ag NPs do not take part of the optical induced reaction in this case. This strategy can be used to decrease D2D and C2C variabilities by controlling the CFs position and minimizing randomness.

On the contrary, UV light was used to perform reset on an Ag NPs@TiO_2-based OEMs device [127] and, in this work, Ag NPs provided the means for an optical set and reset. An additional absorption peak in the visible region, not observed in the TiO_2 film, was found with the introduction of Ag NPs. Both visible light and UV irradiation caused an immediate current increase when the device was on the HRS. As can be seen in figure 5(e), when visible light was turned off, the device gradually decreased its current and stabilized in a state higher than the initial state (HRS) -indication of PPC effect. During UV irradiation, the current would also increase similarly to the previous described study. However, after UV was turned off, the current decreased to a lower conductance state than the HRS (figure 5(f)). This light induced set and reset was related to an oxidation and reduction of Ag NPs, respectively. As schematically illustrated in figure 5(g), under visible illumination, hot electrons would be excited within the Ag NPs through the localized surface plasmon resonance effect and would hop to the conduction band of TiO_2, leaving positively charged Ag^+. This charge separation would induce an oxidation of Ag NPs and decrease the Schottky barrier at the Ag/TiO_2 interface, increasing the current state. On the other hand, UV light irradiation would promote the creation of electron-holes pairs in TiO_2. The resulting free electrons would then react with Ag, reducing the Ag^+ to Ag^0, increasing the Schottky barrier and decreasing the current state.

One-dimensional structures were also coupled with perovskites materials [128–131] for enhanced OE features. In most cases, an abrupt behavior on RS was reported and UV light was used to decrease V_{Set} and V_{Reset}.

Undoubtedly, meaningful attempts have been made in understanding how one can use 1D-structures coupled with other materials to manipulate light-induced RS and achieve photonic set and reset operations. A summary of the most relevant works, and its figures of merit, on this topic is provided in table 4. Once again, IR light provoked RS has the smallest percentage on the works reported, as can be seen in figure 5(h).

It is noticeable, however, that the physical mechanism of RS behavior under light on nanostructured materials still requires clarification for further progress. One NR/NW/NRi can be considered as a single device as a means to fully understand the light interaction with the material in these nanostructures. However, manipulating the RS behavior still poses as a challenge since this type of memristors usually suffer from poor retention and endurance related to Joule heating, high C2C variability and high operating voltages [118, 132]. As an alternative, a network of the nanostructures can be considered as a single device or as an array of devices. The second approach could offer incredible high-density integration since the nanostructured network could be organized in a crossbar configuration. As a prospective example, core–shell NRs could be employed as both bottom and top contacts and single memristor cells would be represented in each crosspoint. The main challenge here is the ordered positioning of the nanostructures [132]. Additionally, the access to single cells would be hard to accomplish due to such small features [118]. Moreover, high D2D variability has been reported for memristors with the smallest areas [2] which can be an indication of how challenging decreasing variability is in single nanostructures. At this point of the research and while effective solutions do not arise to all the above challenges, NPs embedded in thin-films as active layer appears to be a more straight-forward approach to take advantage of nanostructured materials to enhance photo-harvesting in OEMs.

2.5. Remarks

All the works analyzed have provided significant developments in the realization of OEMs using light as an additional input to modulate RS behavior. Both analog and abrupt-RS can be obtained by engineering all sort of material structures. Therefore, it is important to keep in mind what is the application envisioned for the development of an OEM with the required features, as will be discussed in the next section.

Table 4. Comparison of OEMs characteristics based on 1D structures. NRs (nanorods); NPs (nanoparticles); NWs (nanowires); NS (nanostructure); QDs (quantum dots); NRis (nanoribbons). N.S.: not specified at the original paper; N.A.: not applicable. Endurance is related to optical induced RS properties.

Active layer	1D Structure	Electrodes	RS behavior	λ_{light} (nm)	Light effect	DC Sweep Set/Reset (V)	I_{LRS}/I_{HRS} ratio	Endurance (cycles)	Electric retention	PPC	References
ZnO	ZnO NRs	FTO/Au	Abrupt	200–2500	Enables switching behavior	4.5/−3	$\approx 1.00 \times 10^1$	N.S.	No	Yes	[120]
ZnO	ZnO NRs	FTO/Ag	Analog	365	Improves I_{LRS}/I_{HRS} ratio Improves endurance	4/−4	N.S.	40	N.S.	Yes	[133]
ZnO	ZnO NRs	FTO/Pt	Analog	310	Increases current	2.5/−2.5	$>1.00 \times 10^2$	N.S.	No	Yes	[122]
ZP	ZP NPs	ITO/Al	Abrupt	380 532 633 785	Decreases V_{Set}	5/-5	3.63×10^8	N.S.	N.S.	N.S.	[123]
PMMA/ZP/ PMMA	ZP NPs	ITO/Al	Analog	380 532 633	Increases current	6/−6	$<1.00 \times 10^2$	N.S.	No	No	[124]
ZnO/PbS/ZnO	PbS QDs	ITO/Al	Analog	356 780	UV performs set IR performs reset	1/−1	$>1.00 \times 10^1$	N.S.	N.S.	Yes	[20]
ZWO_4	ZWO_4 NWs	Ti/Ag	Abrupt	400–760	Increases I_{LRS}/I_{HRS} ratio	6/−6	$\approx 3.0 \times 10^1$	N.S.	N.S.	N.S.	[134]
$SnWO_4$	$SnWO_4$ NPs	FTO/Ag	Abrupt	400–760	Adds intermediate state	1/−2	$\approx 1.00 \times 10^2$	100	$>5.00 \times 10^2$	N.S.	[135]
$Ce_2W_3O_{12}$	$Ce_2W_3O_{12}$ NS	FTO/Ag	Abrupt	400–760	Adds intermediate states	3/−3	$\approx 1.00 \times 10^1$	50	N.S.	N.S.	[136]
$CuCr_2O_4$	$CuCr_2O_4$ NPs	FTO/Ag	Abrupt	400–760	Adds intermediate states	1/−1	$\approx 1.00 \times 10^3$	100	N.S.	N.S.	[137]
Cu_3P	Cu_3P NRis	ITO/Ag	Abrupt	660	Increases current	−1.5/3	$>1.00 \times 10^3$	N.S.	1.00×10^4	Yes	[138]
Sb_2Se_3/CdS	Sb_2Se_3/CdS NRs	$MoSe_2$/ITO	Abrupt	650	Increases current	1/−0.5	5.00×10^1	3000	2.00×10^4	Yes	[125]
AMT (Ag @Mxene-TiO_2)	Ag NPs	ITO/Au	Abrupt	375	Adds intermediate state	5/−5	$<1.00 \times 10^2$	N.S.	5.00×10^3	Yes	[126]
Ag-TiO_2	Ag NPs	FTO/Au	Abrupt	350 532	Green performs set UV performs reset	2/−2	N.S.	N.S.	$>1.00 \times 10^3$	Yes	[127]

Metal oxide-based OEMs, in their majority, show abrupt RS with sufficient retention time well-suited for digital processing in-memory architecture. For such application, the PPC decay should be suppressed for large enough time, hence, any charge/ion drift destructing the stored state can arise an issue. As shown in the tables above, especially for 2D-materials based OE RS devices, IR light has been demonstrated to induce reset in some cases. IR induced RS is very appealing for wireless systems to enable conversion and storage of IR data. However, for the realization of completely wire-free systems, both set and reset operations need to be performed by light.

Semiconductor oxides and 1D-structured materials as switching medium in OEMs have already shown desirable photonic behavior. Here, strategies such as double-layered thin films with different oxygen contents to arrange a dynamic equilibrium between ionization and neutralization of defects can be applied. In this case, a high energy wavelength can be used to set the device into a saturated photocurrent and then a low energy wavelength can promote the neutralization of defects performing reset. Moreover, the combination of thin films with nanostructured materials such as QDs or NPs can also be employed for a photonic approach. 2D-materials such as graphene can also be coupled with nanostructures such Au NPs for an enhancement of the photocurrent as already shown for a three-terminal device [139].

The switching speed was expected to be enhanced in optical induced transitions, especially for 2D-based or nanostructured OEMs. However, from the available literature this is not yet noticeable. One of the reasons is the immaturity of the technological concept, which leads to most of the reported devices having common bottom contact and not ready for further investigations. However, the switching speed improvement should be a top priority in future developments.

To tackle high performance, OE devices based on metals of nanometer dimension should be also investigated, which has not been explored yet. As can be seen in [140], the performance in terms of switching speed and retention is superior than bulky systems where slow-driving physical mechanisms are dominant. However, one restriction of the pure metallic device concept relies on miniaturization, where maintaining compositional integrity is difficult at reduced dimensions.

If the PPC effect is suppressed in favor of sufficient retention time, DNN applications can be targeted. On the other hand, PPC decay can be further investigated in the scope of SNNs systems. In this regard, short term and long-term memory and time notion should be realized. Time encoding based on optical stimulus turns the system into an event-driven network which favors power efficiency and allows the computational machine to become a truly scalable SNN hardware with yet unexplored computational capabilities [140].

3. OEMs beyond the device level

OEMs have tremendous potential for the development of AI hardware. Since these devices can realize computing in different forms depending on their single-cell characteristics, new possible applications are constantly being trialed.

To be integrated in circuits, novel architecture models should be envisioned as a matrix of OEMs, forming as many synapses as possible, processing element inputs, with built-in auxiliary electronics inspired by pixel circuit, forming an artificial optical neuron.

The advantage of dense circuits and high-speed optics can be realized if the program/write operation takes place in the optical domain and followed by an electrical read-out signal. However, for different applications such as DNN or SNN, various electrical components are required to be considered such as photovoltaic devices and photodetectors to convert/revert electrical/optical signals.

For instance, plasmonic OEMs with the possibility of optical read-out have been proposed. For this purpose, conductive-bridge memristors were developed in which metallic CFs are responsible for RS behavior. In such, when the device is at LRS, metallic CFs block the passage of light whereas at the HRS, light can easily reach a detector [141, 142]. Other studies have shown an optical read using the photovoltaic effect [143, 144].

Light emitting memristors (LEMs) have been developed that can be used for an optical read and write-strategy [145]. Moreover, these light emitting devices can be used as optical communication between layers in ANNs without the need of external light sources. Zhu *et al* proposed a OE artificial nerve composed of LEM layers in which the optical output of one layer was transmitted to the next layer, while simultaneously realizing dynamic adjustable transmissions [146].

Therefore, light stimulus can be used in different strategies to propel the development of an efficient ANNs hardware. On the neural network itself, light input can modulate the synaptic weight update, which corresponds to the conductance state of the memristor. In this case, OEMs can accomplish a variety of synaptic functions bringing us closer to a brain-inspired AI technology. In the next sections of this paper, a review on the already demonstrated capabilities of inorganic OEMs regarding logic gates, neuromorphic functions and, in more detail, artificial visual systems is presented.

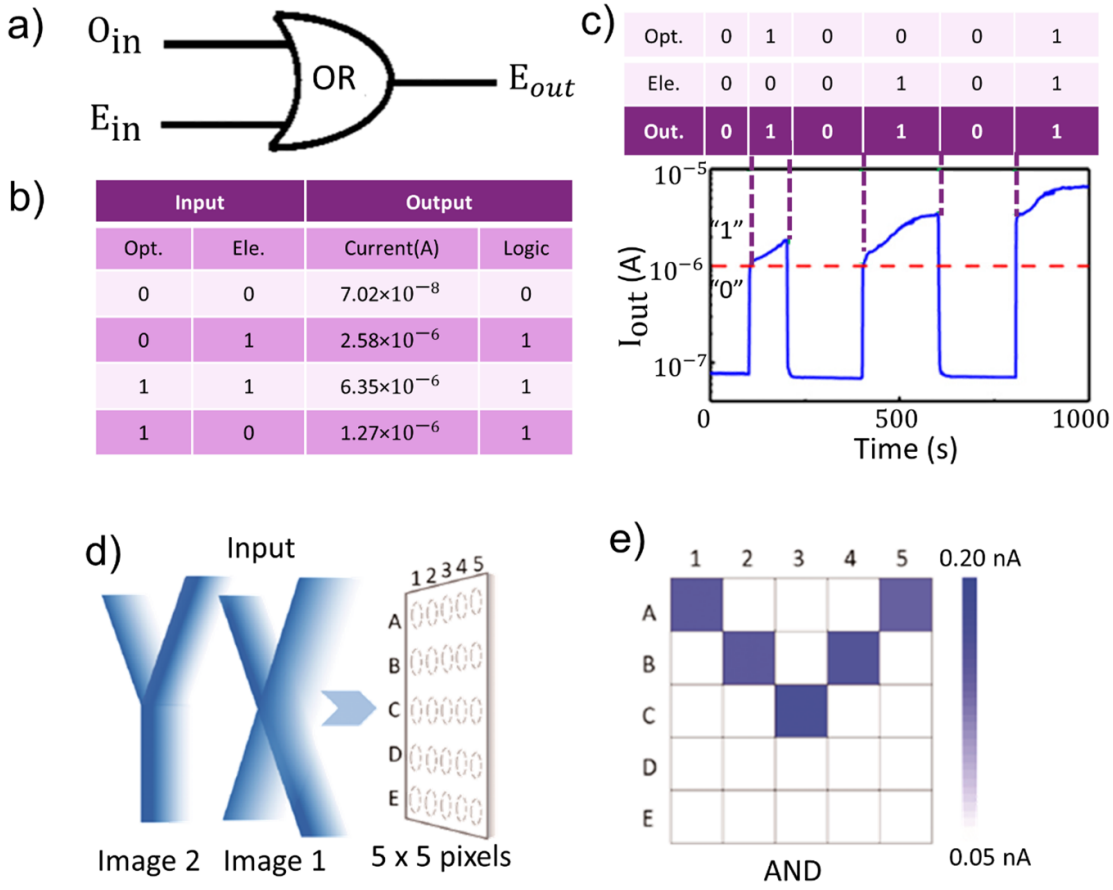

Input		Output	
Opt.	Ele.	Current(A)	Logic
0	0	7.02×10^{-8}	0
0	1	2.58×10^{-6}	1
1	1	6.35×10^{-6}	1
1	0	1.27×10^{-6}	1

Figure 6. Typical OR and AND logic gates. (a) Schematic illustration of OR gate with two inputs, one optical (O_{in}) and one electric (E_{in}), and one electric output (E_{out}). Reprinted from [147], with the permission of AIP Publishing. (b) OR truth table displaying experimental E_{out} values of an OEM and (c) respective E_{out} measured in time for different OR gate combinations. Reprinted [adapted] from [147], with the permission of AIP Publishing. (d) Two images were inputted through visible light in the form of letters Y and X when the devices in a 5 × 5 matrix were in (e) the HRS for an AND gate. Reprinted with permission from [81]. Copyright (2017) American Chemical Society.

3.1. Arithmetic units and Boolean logic

Boolean logic is a form of algebra based on the truth possibilities of true or false that correspond to logic 1 or 0. OEMs can exhibit different non-volatile resistance states at different light wavelengths irradiation, which allows for logic gates and arithmetic functions to be employed. This approach enables in-memory computation which is a significant enhancement from the conventional logic gates based on volatile switches such as transistors, where extra power consumption and time are required due to the physical separation of storage and processing units.

AlO_y/CeO_2 OEM in which four different resistance states could be realized using blue and green irradiation with different intensities (4 and 6 pW μm^2), enabling information storage of 8-bit codes, was reported by Tan *et al* [80]. Broadband light irradiation also showed an increase of current state dependent on light intensity with a retention of state demonstrated for 10^4 s. Moreover, a linear relation between resistance state and number of light pulses was used to employ counter and adder arithmetic functions.

Moreover, an OR gate can be accomplished by OEMs [61, 70, 71], in which a light pulse is used as input A, with 0 corresponding to no light and 1 to irradiation, and an electric pulse as input B, with 0 corresponding to 0 V (or to the read voltage) and 1 corresponding to an input voltage value of X V, in which $X > 0$ V (or the read voltage) and depends on the device's material structure and its set voltage, as schematically illustrated in figure 6(a)). The output should be 1 when A or/and B is at 1 state. In figures 6(b) and (c), an experimentally demonstration of an OR gate is presented, relating to an OEM of structure FTO/$BiVO_4$/TiN [147]. The authors defined the optical input as 1 when the device was irradiated with laser of 405 nm and 11 pW μm^{-2} and the electric input 1 was not described in the original work. A threshold value of current (10^{-6} A) was decided and, therefore, a current output below 10^{-6} A is logic 0 and above 10^{-6} A is logic 1. PPC effect was not shown, which significantly hinders applications where light-induced state storage is necessary. OEMs that can respond to multiple light wavelengths with some degree of retention are preferred.

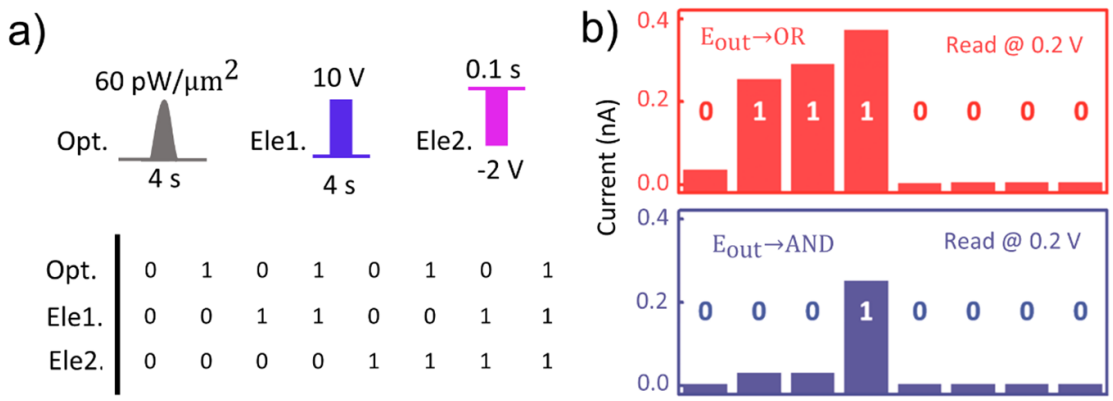

Figure 7. Example of NOT operation in OEMs. (a) Schematic illustration of three possible inputs comprising one optical (O_{in}) and 2 electric (E_{in1} and E_{in2}) and one electric output (E_{out}). E_{in2} was used to reset the device and perform NOT. Truth table of logic operations (AND, OR, AND with NOT and OR with NOT. (b) Experimental results of AND and AND reformatted with NOT operation (in blue) and OR and OR reformatted with NOT operation (in red). Reprinted (adapted) with permission from [81]. Copyright (2017) American Chemical Society.

In this regard, an AND and OR logic gate has been employed in a single cell by OEMs [79, 89]. Light and electric pulses are inputs A and B with 0 and 1 possibilities. Contrary to the OR gate, in the AND gate the output should be 1 only when both inputs A and B are 1. Wang *et al* demonstrated an AND logic gate in which red light was used as input A with a low energy consumption of 4.503 nJ [79]. Red light irradiation by itself could not increase the current state to the defined output logic 1 ($I_{output} > 400$ nA). Therefore, the output logic value was 1 only when the electric input was 1 (4 V with current compliance (CC) set to 1 μA) and the optical input was 1 (red light irradiation). Additionally, using the same device, blue light irradiation could be used for an OR gate with an energy consumption of 4.526 nJ. Blue light illumination supplied enough energy to increase the current state to above the threshold value defined to the output 1 ($I_{output} > 400$ nA). Moreover, the electric input (input B) for the OR gate was defined as 1 for a 4 V input with higher CC than the AND gate (1 mA) to ensure that only the combination of both logic inputs 0 would result in the logic 0 output.

In a different approach, a 5×5 array was constructed to perform logic optoelectronic AND and OR gates. In this experiment, schematically illustrated in figure 6(d), two images were introduced by visible light ($\lambda = 600$ nm for 4 s) in the form of letter Y and X for both AND and OR gates. In this case, both logic inputs are optical (letter Y and X). The AND gate could be realized when all OEMs in the crossbar were in HRS before light irradiation, since only the cells irradiated twice would show an increase of current state to above the threshold value, as can be seen in figure 6(e). The OR gate was in place when all devices in the crossbar were in LRS before irradiation, since the output current of all cells irradiated at least once would increase to above the threshold defined to output logic 1. The results showed an accurate output, proving these crossbar logic OE operations could be applied in larger scales for image processing and storage [81].

NOT operation is also indispensable to the spanning set of a complete logic vector space. Tan *et al* showed NOT operation with an electric pulse that performed reset [81]. In this work, a complex logic design was proposed that comprised an AND gate when input A (light) and input B (electric set) were applied. This AND gate could be reconfigured to an OR gate by applying an additional light pulse before inputs A and B. To perform NOT, an additional electric pulse for reset was applied after inputs A and B, deleting the information encoded, as illustrated in figure 7(a). The experimental results can be consulted in figure 7(b) and show that this strategy can accurately perform these operations. Additionally, optical adder and digital-to-analog converter functions were realized by employing two light pulses as inputs. These light inputs can be combined into binary digital inputs in 00, 01, 10, 11 forms, in which 0 corresponds to dark and 1 corresponds to light irradiation. The current output will be the analog addition of the equivalent of the inputs.

More complex logic gates were also demonstrated such as IMP using two OEMs in series with a conventional resistor in a more complex strategy. NAND could also be observed using blue light [74]. In a recent work, all possible 16 logic functions were realized in a single cell ZnO OEM [90]. However, except for the OR and NIMP functions, a control light had to employed to experimentally demonstrate the other 14 logic functions which ultimately means two light inputs in different sequences for each specific function.

Although these works provide efficient methods for complicated operations using OEMs, the proposed system strategies are somewhat complex utilizing several inputs as part of the operations procedure. In

table 5, a summary of the demonstrated logic gates and arithmetic functions by OEMs can be consulted. It is important to note that Boolean logic is not the only approach to construct integrated circuits that perform mathematical operations. A programmable fuzzy-logic gate approach was proposed as a simpler alternative, in which negative pulses would not be necessary for NOT operation [148], using an OEM that performed material nonimplication and logical true operations using light and electric stimulus.

3.2. In-memory and neuromorphic computation

A range of synaptic functions can be emulated by memristors using their resistance levels as synaptic weights. A non-volatile gradual increase in the memristor conductance state is usually called potentiation, which translates into a higher synaptic weight and simulates the connection between two neurons becoming stronger. On the contrary, depression is when the conductance states decrease related to a lower synaptic weight, which happens as the connection of two neurons become weaker. Therefore, memristive crossbars have been proposed as an alternative to realize ANNs, on hardware in a highly energy, cost and fast efficient manner. OEMs, with their additional light stimulus, can further enhance the advantages reported for neuromorphic computing. Since it is physically separated from the memristor's electrodes, light can act as non-invasive write input to train synaptic weights in crossbars [149, 150].

DNNs are used in several tasks such as pattern recognition, speech recognition or machine translation [151]. In memristor-based DNNs, crossbars perform vector-matrix-multiplication operations (VMMs) as the result of Ohm's and Kirchhoff's summation laws [152], as schematically illustrated in figure 8(a)). The input data is applied as a voltage/current vector at the rows and the output can be read at the columns [153]. These crossbars usually suffer from sneak-path current issues, which are related to electric interference between cells, since all the memristors are connected to each other through conducting wires [154]. A transistor in each cell can be added as a selector element [24, 155, 156], however, it increases energy consumption and cell area. In photonic crossbars, light as an alternative strategy could solve this problem in an energy efficient manner.

A DNN composed of ZnO-based OEMs to perform pattern recognition [89] was proposed by Wang *et al.* A simulation was carried out using potentiation and depression experimental results using input, hidden and output layers composed by 1024, 256 and 15 neurons, respectively. The potentiation and depression were demonstrated using visible light pulses and electric pulses, correspondingly, with a ratio of 25. Based on the back-propagation algorithm simulation, 15 input images were trained in the DNN and after 1000 epochs, the recognition rate was of 86.7%, demonstrating excellent potential. To our knowledge, this work reports on the highest POT/DEP ratio achieved by an OEM so far. However, it still does not quite reach the requirement of 10^2 ratio to ensure less impact of noise in the measurement [157]. Another ZnO-based OEM suited for DNNs was proposed and simulated for pattern recognition as depicted in figure 8(b). All-photonic potentiation and depression was demonstrated using visible light inputs and a pattern recognition accuracy of more than 90% was achieved (figures 8(c) and (d)) [90]. However, potentiation/depression ratio was only 3.2 which is very low for real implementation.

In fact, very few works related to OEMs report on DNNs applications. Not only because of the high ratio requirement but also due to the unwavering criterion of long retention data [157]. As evidenced by the previous sections of this review, this long light-induced current retention is possible with suppression of PPC decay. However, a controlled PPC decay effect by temporal light stimulus is much more useful for SNNs.

The exploration of the PPC effect to emulate SNN related synaptic functions was first proposed by Lee *et al* using planar AOS-based memristors [158]. Since then, several works have followed the trend using vertical OEMs. For instance, using different long enough irradiation time (not light pulses <1 s), Wang *et al* showed the transition from short-term plasticity (STP) to long-term plasticity (LTP) as can be seen in figure 9(a) [125]. The irradiation time affected the PPC dynamic. In the biological system, STP usually last from seconds to dozens of minutes whereas LTP can be determined by hours-weeks or even a life-time of no memory loss [159]. Another way to realize the transition from STP to LTP is by increasing light power, as can be seen in figure 9(b) [160]. A schematic illustration of the multistore memory model is presented in figure 9(c) [161]. As can be perceived, the transition from STP to LTP should be performed by repetition (rehearsal) which can be accomplished by increasing the frequency of light pulses. An example is presented in figure 9(d) [30].

In fact, by continuously irradiating an OEM, the device will suffer a learning process [116, 138]. In figure 9(e), a learning and forgetting test is presented from a double layer ZnO/HfO_x based memristor [160]. During the first learning/forgetting stage, the synaptic weight increases during a 7 s long UV illumination and then, when the light is turned off, gradually decreases (PPC effect) to an intermediate state. Once the light is turned on again, only 4 s are required for the device to return to the synaptic weigh achieved with the first leaning, which shows faster re-learning. Moreover, the retention ratio also increases from 52% to 74% in the second process, showing harder forgetting. The learning and forgetting synaptic function can also be

Table 5. Description of logic gates realized with OEMs and its characteristics. N.S.: not specified at the original paper; N.A.: not applicable; BB: Broadband. I_{LRS}/I_{HRS} ratio is related to the maximum ratio accomplished by light irradiation.

Structure	Size (μm^2)	λ_{light} (nm)	$P_{light\ pulse}$ (mW cm^{-2})	$W_{light\ pulse}$ (s)	I_{LRS}/I_{HRS} ratio	Logic gate /Arithmetic function	PPC	Reference
$Al/AlO_y/CeO_{2-x}/ITO$	7.85×10^3	400–800 499 560	VIS 0.40, 0.60, 6.00 BB 0.08, 2.10, 6.00	3.00	VIS $\approx 3.00 \times 10^2$ BB $\approx 1.00 \times 10^3$	Counter Adder	Yes	[80]
FTO/PVA/SPTP/Ag	N.S.	365	1.00	N.S.	$>1.00 \times 10^1$	Adder OR	No	[71]
$FTO/BiVO_4/TiN$	7.85×10^3	405	1.10	N.S.	$>1.00 \times 10^1$	OR	No	[147]
ITO/ZnO/Ag	4.00×10^4	400–700	N.S.	1.00	$>1.00 \times 10^1$	AND OR	Yes	[89]
$N\text{-}Si/Ta_2O_5/Ta_2O_{5-x}/Ag$	5.03×10^3	460 620	7.00	0.40	$>1.00 \times 10^3$	AND OR	Yes	[79]
$Al/AlO_y/CeO_{(2-x)}/ITO$	7.85×10^3	600	6.00	4.00	$>1.00 \times 10^1$	Adder AND OR NOT	Yes	[81]
$p\text{-}Si/HfO_2/Pt$	1.26×10^3	450	7.96×10^{-4}	N.A.	$>1.00 \times 10^4$	IMP NAND OR	No	[74]
Pt/ZnO/Au	7.85×10^3	530 650	3.60×10^{-2}	N.S.	$>1.00 \times 10^2$	ALL	Yes	[90]

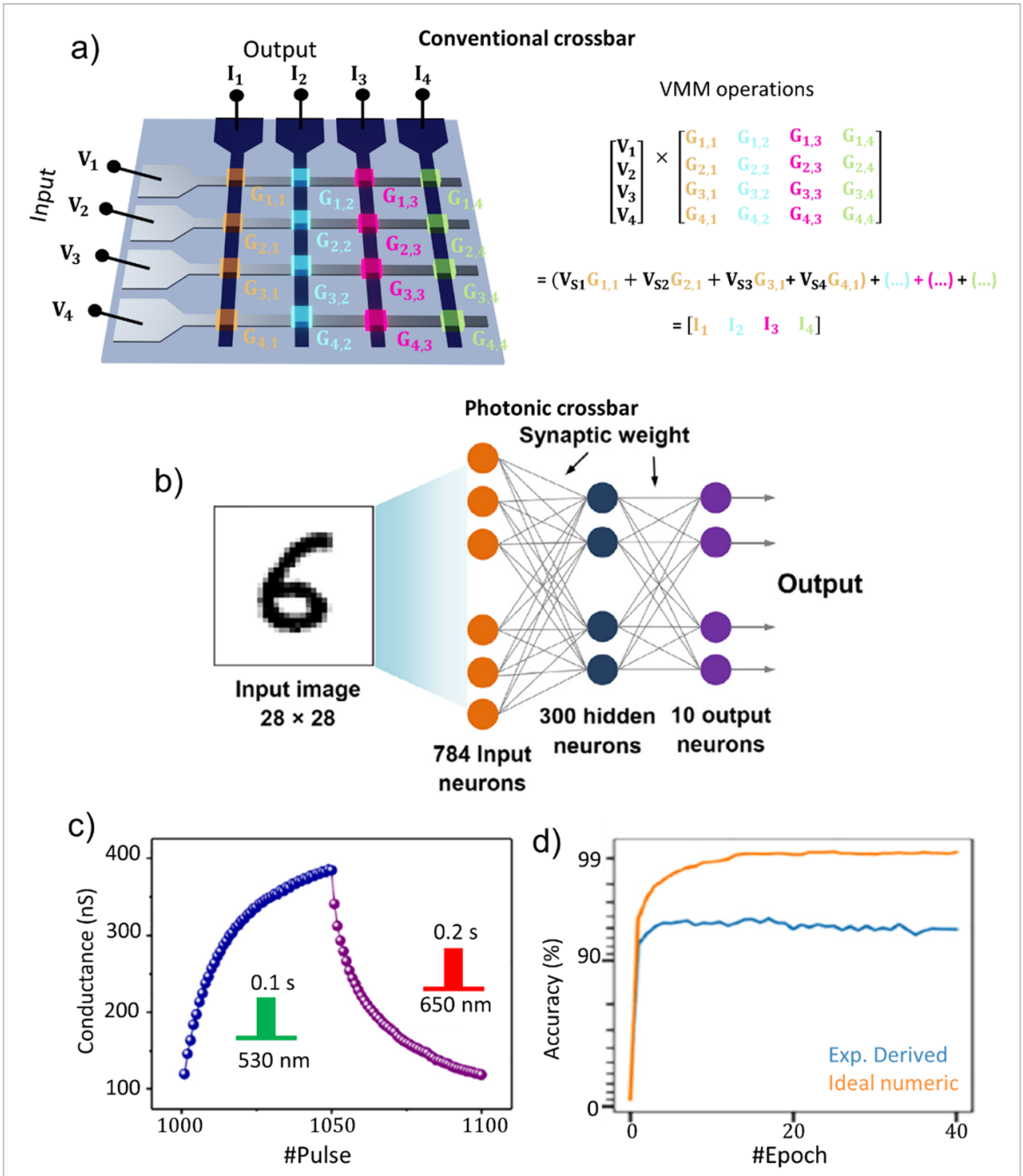

Figure 8. Example of DNNs features using OEMs. (a) Schematic illustration of a 4 × 4 conventional memristive crossbar and corresponding VMM operations. (b) Illustration of a pattern recognition simulation based on a photonic memristive crossbar. DNN composed of 784 input neurons, 300 hidden neurons and 10 output neurons, connected by OE synapses. (c) Experimental optical potentiation and electric depression test realized by green and red light pulses displaying possible synaptic weights to be implemented in the DNN. (d) Recognition rate of simulated DNN for pattern recognition. Reproduced from [90]. CC BY 4.0.

demonstrated under light pulses which is more realistic for future energy-efficient applications, instead of a constant illumination method [99].

Another common synaptic function is paired-pulse facilitation/depression (PPF/PPD). The PPF/PPD index is calculated as the relative current state difference between single and double spikes ((I2–I1)/I1) with the same power and width, yet different intervals between double pulses [77, 87, 101]. An experimental demonstration of PPF can be consulted in figure 9(f), related to a Mo/Sb_2Se_3/CdS/ITO OEM and 650 nm light pulses [125]. PPD was also reported regarding an OEM in which potentiation was performed electrically and depression in a combination of electric pulses and constant optical input [109].

A more complex synaptic function is spike-time dependent plasticity (STDP), key performance applied in SNN models. Here, the synaptic weight change (ΔW) is modulated by the time difference between pre and post-synaptic spikes. As an example, Song *et al* designed a pulse scheme strategy for STDP using two OEMs [103]. The pre-synaptic light spike was applied to one of the devices and the post-synaptic light spike

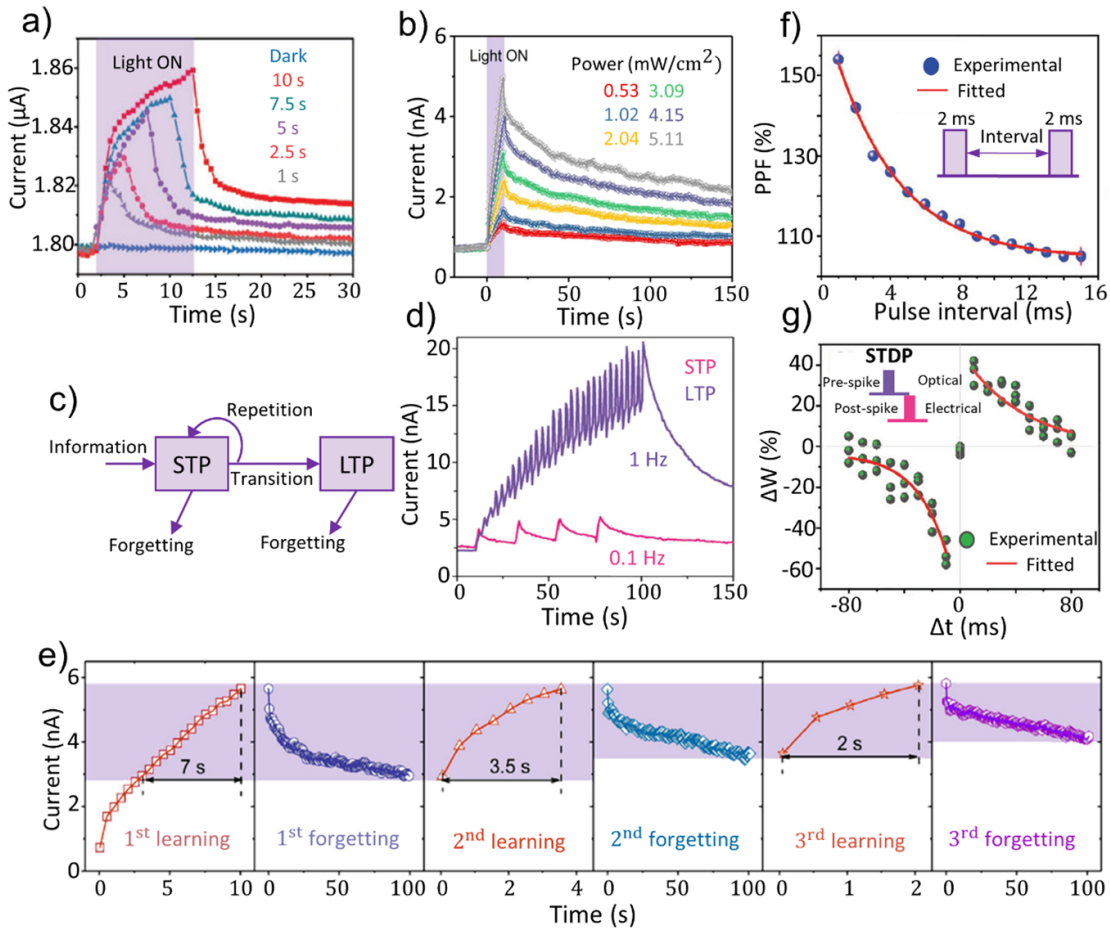

Figure 9. SNNs synaptic functions performed by OEMs. (a) Synaptic weight increase under 3.58 mW cm^{-2} of UV light with different irradiation time, followed by the PPC decay, displaying the transition between STP to LTP. [116] John Wiley & Sons. [© 2021 Wiley-VCH GmbH]. (b) Synaptic weight increase under different power of UV light, followed by PPC decay, displaying transition between STP to LTP. Reprinted [adapted] from [160], with the permission of AIP Publishing. (c) Schematic illustration of the multistore memory model, showing transition from STP to LTP trough repetition (rehearsal). (d) Experimental transition from STP to LTP trough different frequencies of optical UV pulses. [30] John Wiley & Sons. [© 2018 WILEY-VCH Verlag GmbH & Co. KGaA, Weinheim]. (e) Photo-induced learning and forgetting experience, displaying an easier re-learning and harder forgetting by sequenced processes. Reprinted [adapted] from [160], with the permission of AIP Publishing. (f) PPF variation with respect to a double light spike with different intervals. (g) STDP- Variation of connection strength (ΔW) between optical pre and electrical post synaptic spikes applied in a vertical OEM as a function of Δt. [125] John Wiley & Sons. [© 2022 Wiley-VCH GmbH].

was applied to the other one. In another work, the pre-synaptic pulse was applied with light and post-synaptic pulse was electrical [125]. The time interval between the two spikes was defined as $\Delta t = t_{pre} - t_{post}$ and the $\Delta W = (\Delta W_2 - \Delta W_1)/\Delta W_1$. In figure 9(g), the experimental results can be seen. ΔW decreases with longer Δt, as expected, which is typical STDP characteristics of biological synapses [21].

Furthermore, brain-inspired synaptic functions were realized in all-photonic memristors [20, 26]. STDP was emulated in an IGZO device using blue light for potentiation and IR light for depression [26]. The transition from STP to LTP and PPF/PPD functions were demonstrated using UV and IR light on a ITO/ZnO/PbS(QDs)/ZnO/Al photonic memristor [20].

The few studies reporting on all-photonic realized synaptic functions uncover the infinite potential of OEM for brain-inspired neuromorphic computation. In table 6, a summary on the synaptic functions of inorganic OEMs is presented. The scaling possibilities of RS devices, together with an all optical controlled strategy for the implementation of different weights in ANNs, suggest that OEMs crossbar implementation could offer an abysmal efficiency improvement over silicon-based technologies [162].

3.3. Artificial visual systems

In the human visual system, eyes collect information through light signals and convert it to electrical pulses, which are then detected by visual neurons and analyzed and memorized by the visual cortex in the brain. Several kinds of artificial visual systems have been proposed that try to emulate this behavior [163, 164]. Usually, in the conventional image processing based on deep learning-based computer visions, an array of

Table 6. Description of synaptic functions realized with inorganic OEMs and its features. N.S.: not specified at the original paper; N.A.: not applicable. POT/DEP ratio is related to the maximum ratio accomplished during potentiation and depression tests.

Structure	Size (μm^2)	λ_{light} (nm)	$P_{light\ pulse}$ ($mW\ cm^2$)	$W_{light\ pulse}$ (s)	$V_{electric\ pulse}$ (V)	$W_{electric\ pulse}$ (ms)	POT	DEP	POT/DEP ratio	Synaptic functions	PPC	References
ITO/ZnO/Ag	4.00×10^4	400–700	N.S.	1.00	−2.00	10	Optical	Electrical	25.0	DNNs	Yes	[89]
Pt/ZnO/Au	7.85×10^3	530 650	0.03	POT 0.10 DEP 0.20	N.A.	N.A.	Optical	Optical	3.20	DNNs	Yes	[90]
Mo/Sb_2Se_3/CdS/ITO	N.S.	650	200	0.02	N.S.	N.S.	Optical	Electrical	50	STP/LTP PPF STDP Learning/Forgetting	Yes	[125]
ITO/MoS_2/Bi_2Se_3@PMMA/Ag	N.S.	790	1.65	Const.	0.50	1	Electrical	Optical / Electrical	≈2.00	PPD	N.A.	[109]
ITO/Cu_3P/Ag	5.03×10^3	660	200 140 80.0	Const.	0.54 0.42 0.39	10	Optical	Electrical	>10.0 <10.0 <10.0	Learning/Forgetting	Yes	[138]
ITO/TiS_3/Al	3.14×10^4	400 530 808	10.0	Const.	0.42 0.39 0.35	10	Optical	Electrical	<2.00	Pavlov's dog	Yes	[115]
ITO/TiN_xO_{2-x}/MoS_2/Al	7.85×10^3	365	3.15	10.0	N.S.	N.S.	Optical	N.S.	N.S.	STP/LTP PPF Learning/Forgetting	Yes	[116]
Pt/TiO_x/Ti	1.96×10^3	465	12.0	0.05–2.00	N.S.	N.S.	Optical	N.S.	N.S.	PPF	Yes	[77]
ITO/ZnO/Ag	7.85×10^3	366	4.60	0.10	N.S.	N.S.	Optical	N.S.	N.S.	STP/LTP PPF	Yes	[88]
Al/AlO_y/ZnO_{1-x}/ITO	7.85×10^3	310	N.S.	1.00	−4.00	10	Optical	Electrical	≈10.0	STP/LTP PPF	Yes	[101]
FTO/ZnO/In_2O_3	N.S.	365	0.40	1.00	−1.00	20	Optical	Electrical	≈2.00	STP/LTP PPF	Yes	[87]

(Continued.)

Table 6. (Continued.)

Structure	Size (μm^2)	λ_{light} (nm)	$P_{light\ pulse}$ ($mW\ cm^2$)	$W_{light\ pulse}$ (s)	$V_{electric\ pulse}$ (V)	$W_{electric\ pulse}$ (ms)	POT	DEP	POT/DEP ratio	Synaptic functions	PPC	References
Al/IGZO/ITO	2.50×10^3	400	0.15	0.25	2.50	10	Optical	Electrical	≈8.00	STP/LTP STDP	Yes	[103]
ITO/ZTO/ITO	1.77×10^4	405	50.0	N.S.	−1.80	0.07	Optical	Electrical	<2.00	PPF Learning/Forgetting	Yes	[99]
ITO/ZnO/HfO_x/Au	3.14×10^4	365	5.11	2.00	−2.00	50	Optical	Electrical	≈10.0	STP/LTP PPF Learning/Forgetting	Yes	[160]
p-Si/MoS_2/W	1.96×10^3	310	0.11	1.00	−8.00	5	Optical	Electrical	≈10.0	STP/LTP PPF	Yes	[30]
Pt/$IGZO_{(HO)}$/$IGZO_{(LO)}$/Au	7.85×10^3	420 800	POT 0.020 DEP 0.024	POT 1.00 DEP 1.00	N.A.	N.A.	Optical	Optical	≈2.00	STDP	Yes	[26]
ITO/ZnO/PbS QDs/ZnO/Al	N.S.	356 980	0.70 800	0.20 0.20	N.A.	N.A.	Optical	Optical	>10.0	STP/LTP PPF/PPD	Yes	[20]

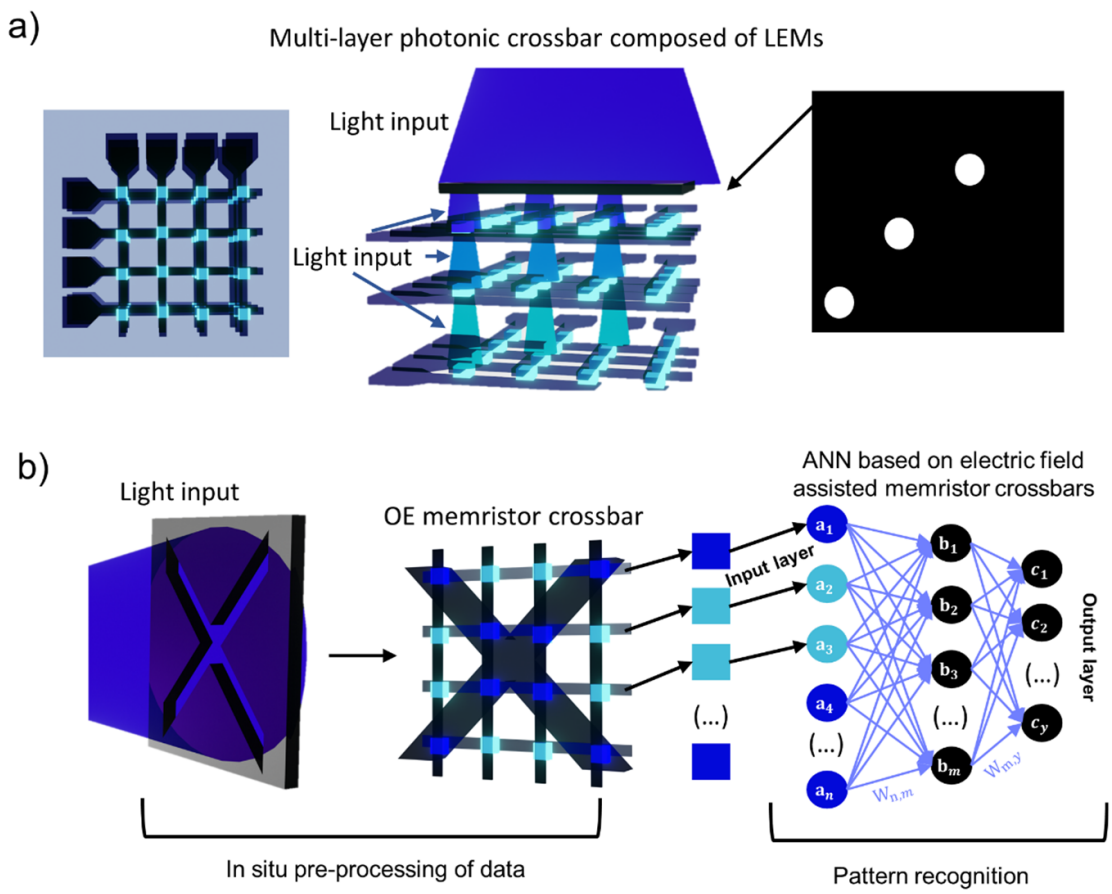

Figure 10. Proposed strategies for the realization of energy efficient artificial visual systems. (a) Illustration of multi-layer photonic crossbar composed of LEMs. (b) Illustration of a photonic crossbar for *in-situ* pre-processing and an ANNs that can be composed of memristors for image recognition.

photodetectors and image sensors are employed, to act as the retina, that gathers light information and converts it to electric signals, transferred to software-based ANN for further processing and storage [165–168]. To improve computer visions, novel algorithms are required to be investigated, especially in the context of human vision-inspired models and SNN approach to synthesize the most realistic image. Furthermore, better sensor performance for long distance and low-light resolution is another research priority in this regard.

OEMs can directly respond to light stimulus and perform light induced synaptic functions, which can simplify the peripheral circuit while offering a more energy and area efficient alternative [169, 170]. Two layers ANNs can easily be realized using crossbars of OEMs, composed of input and output layers, and has already been simulated several times with high pattern recognition accuracies [102, 116, 160, 171], proving the outstanding potential of this approach. However, using photocurrent and light intensity as synaptic weigh modulator in a more complex ANN, with several hidden layers, is a hard to surpass challenge [66]. The light irradiation that inputs on the first layer of the neural network cannot be cascaded into the following layers, unless the already reported strategy on LEM is in place. In such, the first layer OEMs emit light to the second layer, as illustrated in figure 10(a) [146]. Even then, VMM operations would be extremely hard to be accomplished with high accuracy, since photonic I_{LRS}/I_{HRS} ratio is usually low (<10). More studies are demanded to increase the memory window.

A combination of OEMs with ANNs electric-field assisted memristors crossbar looks closer to the reality of today's technology development and can be considered as an effective way to construct an artificial visual system, as illustrated in figure 10(b)). An OE memristive crossbar can be used for a primary *in-situ* processing and image sensing, acting as a neuron that then transfers this information to an electronic-based memristive crossbar, where the processing and storage of this data would take place. In this way, high accuracy recognition tasks can be performed and the overall performance of artificial visual systems would be greatly enhanced [66, 78]. Moreover, using PPC decay on the photonic crossbar can be an efficient way to, on one hand, store the input image for some time (sufficient for inference), and, on the other hand, maintain low power operation due to auto-resetting of the system following relaxation time. Synaptic functions could

also be applied and the whole system could undergo learning processes, in which the more times an image is inputted, the harder it gets for the photonic crossbar to 'forget it'.

4. Conclusion

In this review, the state of the art in inorganic OEMs is described and analyzed. Since the development of these devices should be carried out with a specific application in mind, due to different performance requirements, both memristor materials and structures with its figures of merit and different applications are covered.

On the materials point of view, metal oxides and 2D-materials based OEMs mostly show abrupt RS, suitable for in-memory computation in logic gates or DNNs. IR irradiation has been used to induce reset, which is very appealing for wireless systems, to enable conversion and storage of IR data. Semiconducting-oxides and 1D-structured materials employed as active layer enabled the realization of fully-photonic devices, in which both set and reset were induced by different light wavelengths. However, in the future, it would be important that further studies on the physical mechanism of light-induced RS, and how to control it, be developed.

In regard to possible applications, the PPC effect induced by light can be used to realize all sort of neuromorphic computing requirements. The logic gates already accomplished using inorganic OEMs are discussed in detail. Moreover, in some cases, the PPC decay was shown to be dependent on irradiation time, intensity, frequency and wavelength which was explored to emulate several synaptic functions, also described in this review. In particular, these synaptic functions can be applied for the construction of a more energy, cost and area efficient artificial visual system. Several approaches have been proposed and are analyzed here. Since the photonic ratio has demonstrated to be low (<10) and due to a lack of an efficient way to optically transfer photo-inputs from one to the next layer in an ANN, a combination of photonic and electric crossbars is suggested to efficiently solve these issues.

Data availability statement

No new data were created or analysed in this study.

Acknowledgments

This work is funded by FEDER funds through the COMPETE 2020 Programme and National Funds through the FCT—Portuguese Foundation for Science and Technology, under the scope of the projects UIDB/50025/2020-2023, LA/P/0037/2020, UIDP/50025/2020, doctoral Grant DFA/BD/8335/2020, individual Call to Scientific Employment Stimulus—4th Edition (2021.03386.CEECIND), the project 'NeurOxide', reference PTDC/NAN-MAT/30812/2017 and the project OPERA, reference 2022. 08132.PTDC of the Associate Laboratory Institute of Nanostructures, Nanomodelling and Nanofabrication—i3N. This work also received funding from the European Community's H2020 program under Grant Agreements 716510 (ERC-2016-StG TREND), 787410 (ERC-2019-AdG DIGISMART), 952169 (SYNERGY, H2020-WIDESPREAD-2020-5, CSA) and 101008701 (EMERGE, H2020-INFRAIA-2020-1). TERRAMETA project has also funded this work and received funding from the Smart Networks and Services Joint Undertaking (SNS JU) under the European Union's Horizon Europe research and innovation programme under Grant Agreement No 101097101.

ORCID iDs

Maria Elias Pereira https://orcid.org/0000-0002-2833-2942
Rodrigo Martins https://orcid.org/0000-0002-1997-7669
Elvira Fortunato https://orcid.org/0000-0002-4202-7047
Pedro Barquinha https://orcid.org/0000-0002-5446-2759
Asal Kiazadeh https://orcid.org/0000-0002-8422-5762

References

[1] Chua L O 1971 Memristor—the missing circuit element *IEEE Trans. Circuit Theory* **18** 507–19
[2] Pi S, Li C, Jiang H, Xia W, Xin H, Yang J J and Xia Q 2019 Memristor crossbar arrays with 6-nm half-pitch and 2-nm critical dimension *Nat. Nanotechnol.* **14** 35–39
[3] von Witzleben M, Hennen T, Kindsmüller A, Menzel S, Waser R and Böttger U 2020 Study of the SET switching event of VCM-based memories on a picosecond timescale *J. Appl. Phys.* **127** 204501

[4] von Witzleben M, Wiefels S, Kindsmüller A, Stasner P, Berg F, Cüppers F, Hoffmann-Eifert S, Waser R, Menzel S and Böttger U 2021 Intrinsic RESET speed limit of valence change memories *ACS Appl. Electron. Mater.* **3** 5563–72

[5] Strukov D B, Snider G S, Stewart D R and Williams R S 2008 The missing memristor found *Nature* **453** 80–83

[6] Lee T S, Lee N J, Abbas H, Lee H H, Yoon T S and Kang C J 2020 Compliance current-controlled conducting filament formation in tantalum oxide-based RRAM devices with different top electrodes *ACS Appl. Electron. Mater.* **2** 1154–61

[7] Banerjee W, Cai W F, Zhao X, Liu Q, Lv H, Long S and Liu M 2017 Intrinsic anionic rearrangement by extrinsic control: transition of RS and CRS in thermally elevated TiN/HfO_2/Pt RRAM *Nanoscale* **9** 18908–17

[8] Carlos E, Kiazadeh A, Deuermeier J, Branquinho R, Martins R and Fortunato E 2018 Critical role of a double-layer configuration in solution-based unipolar resistive switching memories *Nanotechnology* **29** 345206

[9] Li T, Yu H, Chen S H Y, Zhou Y and Han S T 2020 The strategies of filament control for improving the resistive switching performance *J. Mater. Chem.* C **8** 16295–317

[10] Lee H Y, Chen P S, Wu T Y, Chen Y S, Wang C C, Tzeng P J, Lin C H, Chen F, Lien C H and Tsai M J 2008 Low power and high speed bipolar switching with a thin reactive Ti buffer layer in robust HfO_2 based RRAM *(San Francisco, CA, USA) 2008 IEEE Int. Electron Devices Meet.* pp 1–4

[11] Bousoulas P, Stathopoulos S, Tsialoukis D and Tsoukalas D 2016 Low-power and highly uniform 3-b multilevel switching in forming free TiO_{2-x}-based RRAM with embedded Pt nanocrystals *IEEE Electron Device Lett.* **37** 874–7

[12] Gul F and Efeoglu H 2017 Bipolar resistive switching and conduction mechanism of an Al/ZnO/Al-based memristor *Superlattices Microstruct.* **101** 172–9

[13] Pereira M, Deuermeier J, Nogueira R, Carvalho P A, Martins R, Fortunato E and Kiazadeh A 2020 Noble-metal-free memristive devices based on IGZO for neuromorphic applications *Adv. Electron. Mater.* **6** 2000242

[14] Pereira M E, Deuermeier J, Freitas P, Barquinha P, Zhang W, Martins R, Fortunato E and Kiazadeh A 2022 Tailoring the synaptic properties of a-IGZO memristors for artificial deep neural networks *APL Mater.* **10** 011113

[15] Casa Branca N, Deuermeier J, Martins J, Carlos E, Pereira M, Martins R, Fortunato E and Kiazadeh A 2020 2D resistive switching based on amorphous zinc–tin oxide Schottky diodes *Adv. Electron. Mater.* **6** 1900958

[16] Silva C, Martins J, Deuermeier J, Pereira M E, Rovisco A, Barquinha P, Goes J, Martins R, Fortunato E and Kiazadeh A 2021 Towards sustainable crossbar artificial synapses with zinc-tin oxide *Electron. Mater.* **2** 105–15

[17] Sawa A and Meyer R 2016 Interface-Type Switching *Resistive Switching: From Fundamentals of Nanoionic Redox Processes to Memristive Device Applications* 1st Edition Ielmini Daniele and Waser Rainer (Hoboken, New Jersey: Wiley) pp 457–82

[18] Dittmann R and Strachan J P 2019 Redox-based memristive devices for new computing paradigm *APL Mater.* **7** 110903

[19] Widrow B and Angell B J 1962 Reliable, trainable networks for computing and control *Aerosp. Eng.* **21** 78–123

[20] Li H, Jiang X, Ye W, Zhang H, Zhou L, Zhang F, She D, Zhou Y and Han S T 2019 Fully photon modulated heterostructure for neuromorphic computing *Nano Energy* **65** 104000

[21] Wang Z Q, Xu H Y, Li X H, Yu H, Liu Y C and Zhu X J 2012 Synaptic learning and memory functions achieved using oxygen ion migration/diffusion in an amorphous InGaZnO memristor *Adv. Funct. Mater.* **22** 2759–65

[22] Ismail M, Abbas H, Choi C and Kim S 2020 Controllable analog resistive switching and synaptic characteristics in ZrO_2/ZTO bilayer memristive device for neuromorphic systems *Appl. Surf. Sci.* **529** 147107

[23] Shi L, Zheng G, Tian B, Dkhil B and Duan C 2020 Research progress on solutions to the sneak path issue in memristor crossbar arrays *Nanoscale Adv.* **2** 1811–27

[24] Pereira M E, Deuermeier J, Figueiredo C, Santos Â, Carvalho G, Tavares V G, Martins R, Fortunato E, Barquinha P and Kiazadeh A 2022 Flexible active crossbar arrays using amorphous oxide semiconductor technology toward artificial neural networks hardware *Adv. Electron. Mater.* **8** 2200642

[25] Emboras A *et al* 2020 Opto-electronic memristors: prospects and challenges in neuromorphic computing *Appl. Phys. Lett.* **117** 230502

[26] Hu L, Yang J, Wang J, Cheng P, Chua L O and Zhuge F 2021 All-optically controlled memristor for optoelectronic neuromorphic computing *Adv. Funct. Mater.* **31** 2005582

[27] Queisser H J and Theodorou D E 1986 Decay kinetics of persistent photoconductivity in semiconductors *Phys. Rev.* B **33** 4027–33

[28] Lee Y C, Shen J L, Chen K W, Lee W Z, Hu S Y, Tiong K K and Huang Y S 2006 Observation of persistent photoconductivity in 2H-Mo Se_2 layered semiconductors *J. Appl. Phys.* **99** 063706

[29] Tebano A, Fabbri E, Pergolesi D, Balestrino G and Traversa E 2012 Room-temperature giant persistent photoconductivity in $SrTiO_3$/$LaAlO_3$ heterostructures *ACS Nano* **6** 1278–83

[30] He H K, Yang R, Zhou W, Huang H M, Xiong J, Gan L, Zhai T Y and Guo X 2018 Photonic potentiation and electric habituation in ultrathin memristive synapses based on monolayer MoS_2 *Small* **14** 1800079

[31] Bernstein J M *et al* 1979 Hail-effect analysis of persistent photocurrents in/i-GaAs layers *Phys. Rev. Lett.* **43** 401–4

[32] Lang D V, Logan R A and Jaros M 1979 Trapping characteristics and a donor-complex (DX) model for the persistent-photoconductivity trapping center in Te-doped $Al_xGa_{1-x}As$ *Phys. Rev.* B **19** 1015–30

[33] Simanjuntak F M, Panda D, Tsai T L, Lin C A, Wei K H and Tseng T Y 2015 Enhancing the memory window of AZO/ZnO/ITO transparent resistive switching devices by modulating the oxygen vacancy concentration of the top electrode *J. Mater. Sci.* **50** 6961–9

[34] Simanjuntak F M, Chandrasekaran S, Lin C C and Tseng T Y 2019 ZnO_2/ZnO bilayer switching film for making fully transparent analog memristor devices *APL Mater.* **7** 051108

[35] Murdoch B J, Raeber T J, Zhao Z C, Barlow A J, McKenzie D R, McCulloch D G and Partridge J G 2019 Light-gated amorphous carbon memristors with indium-free transparent electrodes *Carbon* **152** 59–65

[36] Yan X, Wang J, Zhao M, Li X, Wang H, Zhang L, Lu C and Ren D 2018 Artificial electronic synapse characteristics of a Ta/Ta_2O_{5-x}/Al_2O_3/$InGaZnO_4$ memristor device on flexible stainless steel substrate *Appl. Phys. Lett.* **113** 013503

[37] Fan L, Chen Y, Liu Q, Chen S, Zhu L, Meng Q, Wang B, Zhang Q, Ren H and Zou C 2016 Infrared response and optoelectronic memory device fabrication based on epitaxial VO_2 film *ACS Appl. Mater. Interfaces* **8** 32971–7

[38] Kathalingam A, Kim H S, Kim S D and Park H C 2015 Light induced resistive switching property of solution synthesized ZnO nanorod *Opt. Mater.* **48** 190–7

[39] Wang W, Panin G N, Fu X, Zhang L, Ilanchezhiyan P, Pelenovich V O, Fu D and Kang T W 2016 MoS_2 memristor with photoresistive switching *Sci. Rep.* **6** 31224

[40] Zhu X and Lu W D 2018 Optogenetics-inspired tunable synaptic functions in memristors *ACS Nano* **12** 1242–9

[41] Liu K, Zhang T, Dang B, Bao L, Xu L, Cheng C, Yang Z, Huang R and Yang Y 2022 An optoelectronic synapse based on α-In_2Se_3 with controllable temporal dynamics for multimode and multiscale reservoir computing *Nat. Electron.* **5** 761–73

[42] Sun L, Wang Z, Jiang J, Kim Y, Joo B, Zheng S, Lee S, Yu W J, Kong B S and Yang H 2021 In-sensor reservoir computing for language learning via two-dimensional memristors *Sci. Adv.* **7** eabg1455

[43] Ye C, Peng Q, Li M, Luo J, Tang Z, Pei J, Chen J, Shuai Z, Jiang L and Song Y 2012 Multilevel conductance switching of memory device through photoelectric effect *J. Am. Chem. Soc.* **134** 20053–9

[44] Huebner C F, Tsyalkovsky V, Bandera Y, Burdette M K, Shetzline J A, Tonkin C, Creager S E and Foulger S H 2015 Nonvolatile optically-erased colloidal memristors *Nanoscale* **7** 1270–9

[45] Ling H *et al* 2017 Light-tunable nonvolatile memory characteristics in photochromic RRAM *Adv. Electron. Mater.* **3** 1600416

[46] Lin Y, Zhang X, Shan X, Zeng T, Zhao X, Wang Z, Kang Z, Xu H and Liu Y 2020 Photo-tunable organic resistive random access memory based on PVP/N-doped carbon dot nanocomposites for encrypted image storage *J. Mater. Chem.* C **8** 14789–95

[47] Liu G, Wang C, Zhang W, Pan L, Zhang C, Yang X, Fan F, Chen Y and Li R W 2016 Organic biomimicking memristor for information storage and processing applications *Adv. Electron. Mater.* **2** 1500298

[48] Song S, Kim J, Kwon S M, Jo J, Park S K and Kim Y 2021 Recent progress of optoelectronic and all-optical neuromorphic devices: a comprehensive review of device structures, materials, and applications *Adv. Intell. Syst.* **3** 2000119

[49] Carlos E, Branquinho R, Martins R, Kiazadeh A and Fortunato E 2021 Recent progress in solution-based metal oxide resistive switching devices *Adv. Mater.* **33** 2004328

[50] Zhao W X, Li Q L, Sun B, Shen Z, Liu Y H and Chen P 2014 White-light-controlled resistive switching effect in [BaTiO 3/γ-Fe_2O_3]/ZnO film *Solid State Commun.* **194** 16–19

[51] Sun B, Li Q L, Zhao W X, Li H W, Wei L J and Chen P 2014 White-light-controlled resistance switching in TiO_2/α-Fe_2O_3 composite nanorods array *J. Nanopart. Res.* **16** 2389

[52] Sun B, Liu Y, Zhao W and Chen P 2015 Magnetic-field and white-light controlled resistive switching behaviors in Ag/[$BiFeO_3$/γ-Fe_2O_3]/FTO device *RSC Adv.* **5** 13513–8

[53] Yang N, Hu C Z, Ren Z Q, Bao S Y, Tian B B, Yue F Y, Xiang P H, Zhong N, Duan C G and Chu J H 2020 Nonvolatile negative optoelectronic memory based on ferroelectric thin films *ACS Appl. Electron. Mater.* **2** 1035–40

[54] Kim D J, Tak Y J, Kim W G, Kim J K, Kim J H and Kim H J 2017 Resistive switching properties through iodine migrations of a hybrid perovskite insulating layer *Adv. Mater. Interfaces* **4** 1601035

[55] Guan X, Hu W, Haque M A, Wei N, Liu Z, Chen A and Wu T 2018 Light-responsive ion-redistribution-induced resistive switching in hybrid perovskite Schottky junctions *Adv. Funct. Mater.* **28** 1704665

[56] Zhao X, Xu H, Wang Z, Lin Y and Liu Y 2019 Memristors with organic-inorganic halide perovskites *InfoMat* **1** 183–210

[57] Zhao X, Wang Z, Li W, Sun S, Xu H, Zhou P, Xu J, Lin Y and Liu Y 2020 Photoassisted electroforming method for reliable low-power organic–inorganic perovskite memristors *Adv. Funct. Mater.* **30** 1910151

[58] Chen Q, Han T, Zeng J, He Z, Liu Y, Sun J, Tang M, Zhang Z, Gao P and Liu G 2022 Perovskite-based memristor with 50-fold switchable photosensitivity for in-sensor computing neural network *Nanomaterials* **12** 2217

[59] Poddar S, Zhang Y, Zhu Y, Zhang Q and Fan Z 2021 Optically tunable ultra-fast resistive switching in lead-free methyl-ammonium bismuth iodide perovskite films *Nanoscale* **13** 6184–91

[60] Luo Z, Pei L, Li M, Zhu Y, Xie S, Cheng X, Liu J, Ding H and Xiong R 2018 Electric field-induced resistive switching, magnetism, and photoresponse modulation in a Pt/$Co_{0.03}Zn_{0.97}O$/Nb:$SrTiO_3$ multi-function heterostructure *Appl. Phys. Lett.* **112** 153504

[61] Cai H, Lao M, Xu J, Chen Y, Zhong C, Lu S, Hao A and Chen R 2019 All-inorganic perovskite Cs_4PbBr_6 thin films in optoelectronic resistive switching memory devices with a logic application *Ceram. Int.* **45** 5724–30

[62] Xie S, Pei L, Li M, Zhu Y, Cheng X, Ding H and Xiong R 2019 Light-controlled resistive switching and voltage-controlled photoresponse characteristics in the Pt/CeO_2/Nb:$SrTiO_3$ heterostructure *J. Alloys Compd.* **778** 141–7

[63] Lv F, Zhong T, Qin Y, Qin H, Wang W, Liu F and Kong W 2021 Resistive switching characteristics improved by visible-light irradiation in a $Cs_2AgBiBr_6$-based memory device *Nanomaterials* **11** 1361

[64] Zhong T, Qin Y, Lv F, Qin H and Tian X 2021 Light-activated multilevel resistive switching storage in Pt/$Cs_2AgBiBr_6$/ITO/glass devices *Nanoscale Res. Lett.* **16** 178

[65] Jaafar A H, Gray R J, Verrelli E, O'Neill M, Kelly S M and Kemp N T 2017 Reversible optical switching memristors with tunable STDP synaptic plasticity: a route to hierarchical control in artificial intelligent systems *Nanoscale* **9** 17091–8

[66] Sun J *et al* 2022 A dual-mode organic memristor for coordinated visual perceptive computing *Fundam. Res.* 1–8

[67] Gao S, Liu G, Yang H, Hu C, Chen Q, Gong G, Xue W, Yi X, Shang J and Li R W 2019 An oxide Schottky junction artificial optoelectronic synapse *ACS Nano* **13** 2634–42

[68] Zhou F, Liu Y, Shen X, Wang M, Yuan F and Chai Y 2018 Low-voltage, optoelectronic $CH_3NH_3PbI_{3-x}Cl_x$ memory with integrated sensing and logic operations *Adv. Funct. Mater.* **28** 1800080

[69] Li Y, Cheng P, Zhou L, Liu Z, Zuo Z, Zhan X and Chen J 2021 Light-induced nonvolatile resistive switching in $Cs_{0.15}FA_{0.85}PbI_{3-X}Br_X$ perovskite-based memristors *Solid State Electron.* **186** 108166

[70] Wu Y, Wei Y, Huang Y, Cao F, Yu D, Li X and Zeng H 2017 Capping $CsPbBr_3$ with ZnO to improve performance and stability of perovskite memristors *Nano Res.* **10** 1584–94

[71] Liu Q, Yue W, Li Y, Wang W, Xu L, Wang Y, Gao S, Zhang C, Kan H and Li C 2021 Multifunctional optoelectronic random access memory device based on surface-plasma-treated inorganic halide perovskite *Adv. Electron. Mater.* **7** 2100366

[72] Ungureanu M, Zazpe R, Golmar F, Stoliar P, Llopis R, Casanova F and Hueso L E 2012 A light-controlled resistive switching memory *Adv. Mater.* **24** 2496–500

[73] Borkar H, Thakre A, Kushvaha S S, Aloysius R P and Kumar A 2015 Light assisted irreversible resistive switching in ultra thin hafnium oxide *RSC Adv.* **5** 35046–51

[74] Chen Y, Zhu S, Wei Q, Xia Y, Li A, Yin J and Liu Z 2018 Light-controlled stateful logic operations using optoelectronic switches based on p-Si/HfO_2 heterostructures *Appl. Phys. Lett.* **112** 063503

[75] Hassan M Y and Ang D S 2019 On-demand visible-light sensing with optical memory capabilities based on an electrical-breakdown-triggered negative photoconductivity effect in the ubiquitous transparent hafnia *ACS Appl. Mater. Interfaces* **11** 42339

[76] More K D, Narwade V N, Halge D I, Dadge J W and Bogle K A 2020 Enhanced performance and reduction in operating voltage of TiO_2 thin film based resistive switching memory under optical stimulus *Physica* B **595** 412339

[77] Huang H, Tang J, Gao B, Wang Y, Li X, Wang Z, Qian H and Wu H 2022 Pt/TiO_x/Ti-based dynamic optoelectronic memristor for neuromorphic computing *(Oita, Japan) 6th IEEE Electron Devices Technol. Manuf. Conf. EDTM 2022* pp 310–2

[78] Zhou F *et al* 2019 Optoelectronic resistive random access memory for neuromorphic vision sensors *Nat. Nanotechnol.* **14** 776–82

[79] Wang W, Yin F, Niu H, Li Y, Seong E and Kim Y 2023 Tantalum pentoxide (Ta_2O_5 and Ta_2O_{5-x}) -based memristor for photonic in-memory computing application *Nano Energy* **106** 108072

[80] Tan H, Liu G, Zhu X, Yang H, Chen B, Chen X, Shang J, Lu W D, Wu Y and Li R W 2015 An optoelectronic resistive switching memory with integrated demodulating and arithmetic functions *Adv. Mater.* **27** 2797–803

[81] Tan H, Liu G, Yang H, Yi X, Pan L, Shang J, Long S, Liu M, Wu Y and Li R W 2017 Light-gated memristor with integrated logic and memory functions *ACS Nano* **11** 11298–305

[82] Tan H, Liu G and Li R-W 2018 Multifunctional optoelectronic device based on resistive switching effects *Recent Development in Optoelectronic Devices* (https://doi.org/10.5772/intechopen.74826)

[83] Park J, Huh D, Son S, Kim W, Ju S and Lee H 2022 Transparent, flexible, and low-operating-voltage resistive switching memory based on Al_2O_3/IZO multilayer *Glob. Challenges* **6** 2100118

[84] Wang Z Q, Xu H Y, Li X H, Zhang X T, Liu Y X and Liu Y C 2011 Flexible resistive switching memory device based on amorphous InGaZnO film with excellent mechanical endurance *IEEE Electron Device Lett.* **32** 1442–4

[85] Xie J, Cheng B, Liu L, Ren S, Liu W, Zhou G, Qin H and Hu J 2019 Light-induced double enhancement of resistive switching and control of ferromagnetism in ZnO film *Mater. Res. Express* **6** 096428

[86] Shih C C *et al* 2014 Resistive switching modification by ultraviolet illumination in transparent electrode resistive random access memory *IEEE Electron Device Lett.* **35** 633–5

[87] Kumar M, Abbas S and Kim J 2018 All-oxide-based highly transparent photonic synapse for neuromorphic computing *ACS Appl. Mater. Interfaces* **10** 34370–6

[88] Subin P S, Midhun P S, Antony A, Saji K J and Jayaraj M K 2022 Optoelectronic synaptic plasticity mimicked in ZnO-based artificial synapse for neuromorphic image sensing application *Mater. Today Commun.* **33** 104232

[89] Wang T Y, Meng J L, Li Q X, He Z Y, Zhu H, Ji L, Sun Q Q, Chen L and Zhang D W 2021 Reconfigurable optoelectronic memristor for in-sensor computing applications *Nano Energy* **89** 106291

[90] Yang J, Hu L, Shen L, Wang J, Cheng P, Lu H, Zhuge F and Ye Z 2022 Optically driven intelligent computing with ZnO memristor *Fundam. Res.* 1–9

[91] Liu H, Zeng F, Lin Y, Wang G and Pan F 2013 Correlation of oxygen vacancy variations to band gap changes in epitaxial ZnO thin films *Appl. Phys. Lett.* **102** 181908

[92] Kiazadeh A, Gomes H L, Barquinha P, Martins J, Rovisco A, Pinto J V, Martins R and Fortunato E 2016 Improving positive and negative bias illumination stress stability in parylene passivated IGZO transistors *Appl. Phys. Lett.* **109** 051606

[93] Kumar D, Saleem A, Keong L B, Wang Y H and Tseng T Y 2022 Light induced RESET phenomenon in invisible memristor for photo sensing *IEEE Electron Device Lett.* **3106** 22–25

[94] Zhou F, Chen J, Tao X, Wang X and Chai Y 2019 2D materials based optoelectronic memory: convergence of electronic memory and optical sensor *Research* **2019** 9490413

[95] Kang B H, Kim W G, Chung J, Lee J H and Kim H J 2018 Simple hydrogen plasma doping process of amorphous indium gallium zinc oxide-based phototransistors for visible light detection *ACS Appl. Mater. Interfaces* **10** 7223–30

[96] Cho K S, Heo K, Baik C W, Choi J Y, Jeong H, Hwang S and Lee S Y 2017 Color-selective photodetection from intermediate colloidal quantum dots buried in amorphous-oxide semiconductors *Nat. Commun.* **8** 840

[97] Kumar D, Shrivastava S, Saleem A, Singh A, Lee H, Wang Y H and Tseng T Y 2022 Highly efficient invisible TaO_x/ZTO bilayer memristor for neuromorphic computing and image sensing *ACS Appl. Electron. Mater.* **4** 2180–90

[98] Retamal J R D, Kang C F, Ho C H, Ke J J, Chang W Y and He J H 2014 Effect of ultraviolet illumination on metal oxide resistive memory *Appl. Phys. Lett.* **105** 253111

[99] Shrivastava S, Lin Y T, Pattanayak B, Pratik S, Hsu C C, Kumar D, Lin A S and Tseng T Y 2022 Zn_2SnO_4 thin film based nonvolatile positive optoelectronic memory for neuromorphic computing *ACS Appl. Electron. Mater.* **4** 1784–93

[100] Mehonic A, Gerard T and Kenyon A J 2017 Light-activated resistance switching in SiO_x RRAM devices *Appl. Phys. Lett.* **111** 233502

[101] Hu D C, Yang R, Jiang L and Guo X 2018 Memristive synapses with photoelectric plasticity realized in ZnO_{1-x}/AlO_y heterojunction *ACS Appl. Mater. Interfaces* **10** 6463–70

[102] Zhou Z, Pei Y, Zhao J, Fu G and Yan X 2021 Visible light responsive optoelectronic memristor device based on CeO_x/ZnO structure for artificial vision system *Appl. Phys. Lett.* **118** 191103

[103] Song S, Kim M, Yoo G, Kwon S M, Heo J S, Park S K and Kim Y H 2021 Solution-processed oxide semiconductor-based artificial optoelectronic synapse array for spatiotemporal synaptic integration *J. Alloys Compd.* **857** 158027

[104] Yan F, Wei Z, Wei X, Lv Q, Zhu W and Wang K 2018 Toward high-performance photodetectors based on 2D materials: strategy on methods *Small Methods* **2** 1700349

[105] Wang M *et al* 2018 Robust memristors based on layered two-dimensional materials *Nat. Electron.* **1** 130–6

[106] Bertolazzi S, Bondavalli P, Roche S, San T, Choi S Y, Colombo L, Bonaccorso F and Samorì P 2019 Nonvolatile memories based on graphene and related 2D materials *Adv. Mater.* **31** 1806663

[107] Sun B, Guo T, Zhou G, Ranjan S, Hou W, Hou Y and Zhao Y 2019 Tunneling of photon-generated carrier in the interface barrier induced resistive switching memory behaviour *J. Colloid Interface Sci.* **553** 682–7

[108] Jaafar A H and Kemp N T 2019 Wavelength dependent light tunable resistive switching graphene oxide nonvolatile memory devices *Carbon* **153** 81–88

[109] Wang Y, Yang J, Wang Z, Chen J, Yang Q, Lv Z, Zhou Y, Zhai Y, Li Z and Han S T 2019 Near-infrared annihilation of conductive filaments in quasiplane $MoSe_2$/Bi_2Se_3 nanosheets for mimicking heterosynaptic plasticity *Small* **15** 1805431

[110] Zhou Y *et al* 2020 Black phosphorus based multicolor light-modulated transparent memristor with enhanced resistive switching performance *ACS Appl. Mater. Interfaces* **12** 25108–14

[111] Zhang Z, Yang D, Li H, Li C, Wang Z, Sun L and Yang H 2022 2D materials and van der Waals heterojunctions for neuromorphic computing *Neuromorphic Comput. Eng.* **2** 032004

[112] Huh W, Lee D and Lee C H 2020 Memristors based on 2D materials as an artificial synapse for neuromorphic electronics *Adv. Mater.* **32** 2002092

[113] Chen Y *et al* 2021 Broadband Bi_2O_2Se photodetectors from infrared to terahertz *Adv. Funct. Mater.* **31** 2009554

[114] Qiu Q and Huang Z 2021 Photodetectors of 2D materials from ultraviolet to terahertz waves *Adv. Mater.* **33** 2008126

[115] Liu L, Cheng Z, Jiang B, Liu Y, Zhang Y, Yang F, Wang J, Yu X F, Chu P K and Ye C 2021 Optoelectronic artificial synapses based on two-dimensional transitional-metal trichalcogenide *ACS Appl. Mater. Interfaces* **13** 30797–805

[116] Wang W, Gao S, Li Y, Yue W, Kan H, Zhang C, Lou Z, Wang L and Shen G 2021 Artificial optoelectronic synapses based on $TiNxO_{2-x}$/MoS_2 heterojunction for neuromorphic computing and visual system *Adv. Funct. Mater.* **31** 2101201

[117] Ding G, Zhou K, Li T, Yang B and Zhou Y 2020 One-dimensional materials for photoelectroactive memories and synaptic devices *Photo-Electroactive Nonvolatile Memories for Data Storage and Neuromorphic Computing* pp 179–200

[118] Milano G, Porro S, Valov I and Ricciardi C 2019 Recent developments and perspectives for memristive devices based on metal oxide nanowires *Adv. Electron. Mater.* **5** 1800909
[119] Lu W and Lieber C M 2009 Nanoelectronics from the bottom up *Nanosci. Technol.* A **6** 841–50
[120] Park J, Lee S and Yong K 2012 Photo-stimulated resistive switching of ZnO nanorods *Nanotechnology* **23** 385707
[121] Park J, Lee S, Lee J and Yong K 2013 A light incident angle switchable ZnO nanorod memristor: reversible switching behavior between two non-volatile memory devices *Adv. Mater.* **25** 6423–9
[122] Zhou W, Yang R, He H K, Huang H M, Xiong J and Guo X 2018 Optically modulated electric synapses realized with memristors based on ZnO nanorods *Appl. Phys. Lett.* **113** 061107
[123] Hu L, Yuan J, Ren Y, Wang Y, Yang J Q, Zhou Y, Zeng Y J, Han S T and Ruan S 2018 Phosphorene/ZnO nano-heterojunctions for broadband photonic nonvolatile memory applications *Adv. Mater.* **30** 1801232
[124] Ren Y, Hu L, Mao J Y, Yuan J, Zeng Y J, Ruan S, Yang J Q, Zhou L, Zhou Y and Han S T 2018 Phosphorene nano-heterostructure based memristors with broadband response synaptic plasticity *J. Mater. Chem.* C **6** 9383–93
[125] Pei Y *et al* 2022 A multifunctional and efficient artificial visual perception nervous system with Sb_2Se_3/CdS-core/shell (SC) nanorod arrays optoelectronic memristor *Adv. Funct. Mater.* **32** 2203454
[126] Guo L *et al* 2021 Stacked two-dimensional MXene composites for an energy-efficient memory and digital comparator *ACS Appl. Mater. Interfaces* **13** 39595–605
[127] Shan X *et al* 2022 Plasmonic optoelectronic memristor enabling fully light-modulated synaptic plasticity for neuromorphic vision *Adv. Sci.* **9** 2104632
[128] Wang Y *et al* 2018 Synergies of electrochemical metallization and valance change in all-inorganic perovskite quantum dots for resistive switching *Adv. Mater.* **30** 1800327
[129] Zhang X, Yang H, Jiang Z, Zhang Y, Wu S, Pan H, Khisro N and Chen X 2019 Photoresponse of nonvolatile resistive memory device based on all-inorganic perovskite $CsPbBr_3$ nanocrystals *J. Phys. D: Appl. Phys.* **52** 125103
[130] Chen Z *et al* 2019 Light assisted multilevel resistive switching memory devices based on all-inorganic perovskite quantum dots *Appl. Phys. Lett.* **114** 181103
[131] Zhou Y, Yew K S, Ang D S, Kawashima T, Bera M K, Zhang H Z and Bersuker G 2015 White-light-induced disruption of nanoscale conducting filament in hafnia *Appl. Phys. Lett.* **107** 072107
[132] Ielmini D, Cagli C, Nardi F and Zhang Y 2013 Nanowire-based resistive switching memories: devices, operation and scaling *J. Phys. D: Appl. Phys* **46** 074006
[133] Russo P, Xiao M, Liang R and Zhou N Y 2018 UV-induced multilevel current amplification memory effect in zinc oxide rods resistive switching devices *Adv. Funct. Mater.* **28** 1706230
[134] Zhao W X, Sun B, Liu Y H, Wei L J, Li H W and Chen P 2014 Light-controlled resistive switching of $ZnWO_4$ nanowires array *AIP Adv.* **4** 077127
[135] Han P, Sun B, Cheng S, Yu F, Jiao B and Wu Q 2016 An optoelectronic resistive switching memory behavior of Ag/α-$SnWO_4$/FTO device *J. Alloys Compd.* **681** 516–21
[136] Sun B, Li X, Liang D and Chen P 2016 Effect of visible-light illumination on resistive switching characteristics in Ag/$Ce_2W_3O_{12}$/FTO devices *Chem. Phys. Lett.* **643** 66–70
[137] Sun B, Wu J, Jia X, Lou F and Chen P 2015 Preparation and light-controlled resistive switching memory behavior of $CuCr_2O_4$ *J. Sol-Gel Sci. Technol.* **75** 664–9
[138] Liu Y *et al* 2022 Topochemical synthesis of copper phosphide nanoribbons for flexible optoelectronic memristors *Adv. Funct. Mater.* **32** 2110900
[139] Liu Y, Cheng R, Liao L, Zhou H, Bai J, Liu G, Liu L, Huang Y and Duan X 2011 Plasmon resonance enhanced multicolour photodetection by graphene *Nat. Commun.* **2** 579
[140] Cheng Z, Milne T, Salter P, Kim J S, Humphrey S, Booth M and Bhaskaran H 2021 Antimony thin films demonstrate programmable optical nonlinearity *Sci. Adv.* **8** 2004185
[141] Emboras A, Goykhman I, Desiatov B, Mazurski N, Stern L, Shappir J and Levy U 2013 Nanoscale plasmonic memristor with optical readout functionality *Nano Lett.* **13** 6151–5
[142] Hoessbacher C, Fedoryshyn Y, Emboras A, Melikyan A, Kohl M, Hillerkuss D, Hafner C and Leuthold J 2014 The plasmonic memristor: a latching optical switch *Optica* **1** 198–202
[143] Xiao Z and Huang J 2016 Energy-efficient hybrid perovskite memristors and synaptic devices *Adv. Electron. Mater.* **2** 1600100
[144] Lu Z, Yang X, Jin C, Li P, Wan J G and Liu J M 2018 Nonvolatile electric-optical memory controlled by conductive filaments in Ti-doped $BiFeO_3$ *Adv. Electron. Mater.* **4** 1700551
[145] Zakhidov A A, Jung B, Slinker J D, Abruña H D and Malliaras G G 2010 A light-emitting memristor *Org. Electron.* **11** 150–3
[146] Zhu Y, Wu C, Xu Z, Liu Y, Hu H, Guo T, Kim T W, Chai Y and Li F 2021 Light-emitting memristors for optoelectronic artificial efferent nerve *Nano Lett.* **21** 6087–94
[147] Zhao J, Zhou Z, Wang H, Wang J, Hao W, Ren D, Guo R, Chen J, Liu B and Yan X 2019 A Boolean or gate implemented with an optoelectronic switching memristor *Appl. Phys. Lett.* **115** 153504
[148] Berco D, Ang D S and Kalaga P S 2020 Programmable photoelectric memristor gates for *in situ* image compression *Adv. Intell. Syst.* **2** 2000079
[149] Mao J Y, Zhou L, Zhu X, Zhou Y and Han S T 2019 Photonic memristor for future computing: a perspective *Adv. Opt. Mater.* **7** 1900766
[150] Mao J Y, Hu L, Zhang S R, Ren Y, Yang J Q, Zhou L, Zeng Y J, Zhou Y and Han S T 2019 Artificial synapses emulated through a light mediated organic-inorganic hybrid transistor *J. Mater. Chem.* C **7** 48–59
[151] Liu X and Zeng Z 2022 Memristor crossbar architectures for implementing deep neural networks *Complex Intell. Syst.* **8** 787–802
[152] Naqi M, Kang M S, Liu N, Kim T, Baek S, Bala A, Moon C, Park J and Kim S 2022 Multilevel artificial electronic synaptic device of direct grown robust MoS_2 based memristor array for in-memory deep neural network *npj 2D Mater. Appl.* **6** 53
[153] Mehonic A, Sebastian A, Rajendran B, Simeone O, Vasilaki E and Kenyon A J 2020 Memristors-from in-memory computing, deep learning acceleration, and spiking neural networks to the future of neuromorphic and bio-inspired computing *Adv. Intell. Syst.* **2** 2000085
[154] Li H *et al* 2021 Memristive crossbar arrays for storage and computing applications *Adv. Intell. Syst.* **3** 2100017
[155] Hu M *et al* 2018 Memristor-based analog computation and neural network classification with a dot product engine *Adv. Mater.* **30** 1705914
[156] Yao P, Wu H, Gao B, Tang J, Zhang Q, Zhang W, Yang J J and Qian H 2020 Fully hardware-implemented memristor convolutional neural network *Nature* **577** 641–6

[157] Moon K, Lim S, Park J, Sung C, Oh S, Woo J, Lee J and Hwang H 2019 RRAM-based synapse devices for neuromorphic systems *Faraday Discuss.* **213** 421–51
[158] Lee M, Lee W, Choi S, Jo J W, Kim J, Park S K and Kim Y H 2017 Brain-inspired photonic neuromorphic devices using photodynamic amorphous oxide semiconductors and their persistent photoconductivity *Adv. Mater.* **29** 1700951
[159] Chang T, Jo S H and Lu W 2011 Short-term memory to long-term memory transition in a nanoscale memristor *ACS Nano* **5** 7669–76
[160] Shan X *et al* 2022 Optoelectronic synaptic device based on ZnO/HfO_x heterojunction for high-performance neuromorphic vision system *Appl. Phys. Lett.* **121** 263501
[161] Brelsford J W and Atkinson R C 1968 Recall of paired-associates as a function of overt and covert rehearsal procedures *J. Verbal Learn. Verbal Behav.* **7** 730–6
[162] Nishitani Y, Kaneko Y and Ueda M 2015 Supervised learning using spike-timing-dependent plasticity of memristive synapses *IEEE Trans. Neural Netw. Learn. Syst.* **26** 2999–3008
[163] Mathieson K *et al* 2012 Photovoltaic retinal prosthesis with high pixel density *Nat. Photon.* **6** 391–7
[164] Kwon S M, Cho S W, Kim M, Heo J S, Kim Y H and Park S K 2019 Environment-adaptable artificial visual perception behaviors using a light-adjustable optoelectronic neuromorphic device array *Adv. Mater.* **31** 1906433
[165] Zhang L, Yu H, Xiao C, Si J, Xu H, Zhu W and Wang L 2021 Building light stimulated synaptic memory devices for visual memory simulation *Adv. Electron. Mater.* **7** 2000945
[166] Chen S, Lou Z, Chen D and Shen G 2018 An artificial flexible visual memory system based on an UV-motivated memristor *Adv. Mater.* **30** 1705400
[167] Xiao C, Xu B, Si J, Di Z, Zhao L, Liu R, Lv Q, Wang L and Zhang L 2022 Wide waveband light detection and storage device for visual memory *Phys. Status Solidi* **219** 2100881
[168] Dang B, Liu K, Wu X, Yang Z, Xu L, Yang Y and Huang R 2022 One-phototransistor–one-memristor array with high-linearity light-tunable weight for optic neuromorphic computing *Adv. Mater.* **2022** 2204844
[169] Tian H, Wang X, Wu F, Yang Y and Ren T L 2018 High performance 2D perovskite/graphene optical synapses as artificial eyes (*San Francisco, CA, USA) IEEE International Electron Devices Meeting (IEDM)* pp 38.6.1–38.6.4
[170] Seo S *et al* 2018 Artificial optic-neural synapse for colored and color-mixed pattern recognition *Nat. Commun.* **9** 5106
[171] Li R *et al* 2023 Multi-modulated optoelectronic memristor based on Ga_2O_3/MoS_2 heterojunction for bionic synapses and artificial visual system *Nano Energy* **111** 108398